energies

MDPI

Review

Electrochemical Mechanism Underlying Lithium Plating in Batteries: Non-Invasive Detection and Mitigation

Sourav Das and Pranav Shrotriya *

Department of Mechanical Engineering, Iowa State University, Ames, IA 50011, USA; sourav1@iastate.edu
* Correspondence: shrotriy@iastate.edu

Abstract: Efficient, sustainable, safe, and portable energy storage technologies are required to reduce global dependence on fossil fuels. Lithium-ion batteries satisfy the need for reliability, high energy density, and power density in electrical transportation. Despite these advantages, lithium plating, i.e., the accumulation of metallic lithium on the graphite anode surface during rapid charging or at low temperatures, is an insidious failure mechanism that limits battery performance. Lithium plating significantly shortens the battery's life and rapidly reduces capacity, limiting the widespread adoption of electrical vehicles. When lithium plating is extreme, it can develop lithium dendrites, which may pass through the separator and lead to an internal short circuit and the subsequent thermal runaway damage of the cell. Over the last two decades, a large number of published studies have focused on understanding the mechanisms underlying lithium plating and on approaches to mitigate its harmful effects. Nevertheless, the physics underlying lithium plating still needs to be clarified. There is a lack of real-time techniques to accurately detect and quantify lithium plating. Real-time detection is essential for alleviating lithium plating-induced failure modes. Several strategies have been explored to minimize plating and its effect on battery life and safety, such as electrolyte design, anode structure design, and hybridized charging protocol design. We summarize the current developments and the different reported hypotheses regarding plating mechanisms, the influence of environmental and electrochemical conditions on plating, recent developments in electrochemical detection methods and their potential for real-time detection, and plating mitigation techniques. The advantages and concerns associated with different electrochemical detection and mitigation techniques are also highlighted. Lastly, we discuss outstanding technical issues and possible future research directions to encourage the development of novel ideas and methods to prevent lithium plating.

Keywords: lithium-ion batteries; fast charging; lithium plating; sensing; low-temperature; state-of-health; damage; mitigation; detection

Citation: Das, S.; Shrotriya, P. Electrochemical Mechanism Underlying Lithium Plating in Batteries: Non-Invasive Detection and Mitigation. *Energies* **2024**, *17*, 5930. https://doi.org/10.3390/en17235930

Academic Editors: Truong Quang Dinh, Cheng Zhang and Truong Minh Ngoc Bui

Received: 1 October 2024
Revised: 7 November 2024
Accepted: 13 November 2024
Published: 26 November 2024

1. Introduction

The conventional transportation and energy sectors are leading contributors to worldwide greenhouse gas (GHG) emissions. The electrification of the transportation sector is proposed as a commercially viable solution to limit GHG emissions and environmental damage [1–3]. The success of the electrification of the automobile sector and the adoption of renewable energy systems depends mainly on the capabilities of the electric energy storage system [4–7]. Metal-ion batteries, such as lithium, sodium, etc., are readily available and proven options for the electro-mobility industry across different vehicle segments [8,9]. Lithium-ion batteries are utilized for electric vehicles because of their high energy density, high power density, light weight, and efficiency [9,10]. Despite these advantages, the lithium-ion battery suffers challenges, such as capacity reduction due to aging, fast charging, limited low-temperature charging, and safety concerns [9,11,12]. More than 130,000 articles on LiBs were published (Figure 1a) up to 2024, suggesting extensive growth in research on and interest in lithium batteries.

Typical lithium-ion cells consist of porous anode and cathode films on metallic current collectors, immersed in an electrolyte and separated by an insulating porous polymeric membrane (separator). Graphite is the most common anode material found in the cell. Other explored anode materials, such as the Li metal anode, are susceptible to rapid dendritic plating, whereas hard carbon has lower electrical conductivity than graphite [13,14]. Another appealing anode material is $Li_4Ti_5O_{12}$ (LTO), which exhibits good cycling stability, quick kinetics, and high-rate capability but lacks electrical conductivity and the diffusivity of lithium ions [15,16]. On the other side, the carbon nanotube (CNT)-based anode has also been used as an alternative in recent years. Still, its application is also limited due to lower electronic conductivity and higher irreversible loss [17]. However, this paper focuses more on the graphite-based anode due to its wide use across the electric vehicle sector. The cathode of lithium-ion batteries is a composite of metal oxides with different microstructures, such as a layer, a spinal, or an olivine tunnel. Lithium ions move from the cathode into the anode during charging, and the electrochemical reactions are reversed during battery discharging [18]. The cathode microstructure and its conductivity also determine the lithium-ion flux, resulting in different areal energy densities [19]. The anode and cathode materials are coated on copper and aluminum films, respectively. A liquid mixture of ionic lithium salts and ethylene carbonate salts is commonly used as an electrolyte medium, and an ion-conductive polymeric separator soaked in the electrolyte acts as an insulating medium between the anode and cathode [13]. A typical lithium-ion battery loses its cyclable capacity during cycling and is limited in its useful life due to several levels of degradation processes, as described in Table 1 [20–32] and schematically depicted in Figure 1b.

Due to the high reactivity of lithium-based salt, $LiPF_6$-based electrolytes are reduced when in contact with graphite anodes, which have a closer open circuit potential and form an ion-permeable and insulative solid–electrolyte interface (SEI) layer on their surface, as shown in Figure 1b. The SEI layer consumes cyclable lithium, causing a cell capacity loss and a rise in cell impedance. The loss in capacity is directly correlated with the thickening of the SEI layers during cycling at low C rates [24,25]. Another anodic degradation is lithium plating; more than one-eighth of the reported publications on battery failure have focused on lithium plating-induced failures. Figure 1c [22,30] schematically represents the composite film of plated lithium and SEI around an anode particle. Plating results in a rapid cyclable capacity loss and coulombic efficiency drop, as shown in Figure 1d. Lithium-ion batteries are also vulnerable to active material loss due to cathode fracture, dissolution, and electrolyte decomposition [24]. Several other stress factors are also responsible for these degradations, such as high-temperature charging, which accelerates the electrolyte's oxidation and releases gases that cause cell swelling [26,27]. In comparison, high C rate charging and the high depth of discharge of the cathode result in cathode fracture and active material dissolution [28]. The aging study of lithium cells also showcases the breakdown of the binder during long cycling tests [29]. Among all these factors, health loss in a lithium battery is mainly dominated by lithium plating.

Table 1. Degradation mechanism in LiBs.

Physical and Chemical Mechanism of Damage	Effect on Battery Performance
Continuous growth of SEI	Loss of cyclable lithium resulting in capacity fade and impedance rise [33].
Lithium plating and electrolyte decomposition	Loss of cyclable lithium ions results in rapid capacity loss [24,26].
Particle cracking and solvent intercalation	Loss of active electrode material and lithium ions showing rapid capacity fade, increase in overpotential [24,34].
Loss in porosity due to irreversible salt deposition	Impedance rises in the cell [24,35].
Delamination and dissolution of electrode material	Loss of active material and capacity fade [36,37].
Decomposition of electrolyte and binder and gas evolution	Loss of cyclable lithium, impedance rise, and capacity fade of the cell [24].
Corrosion of current collector	Impedance rises and inhomogeneous current-voltage distribution [24,38].

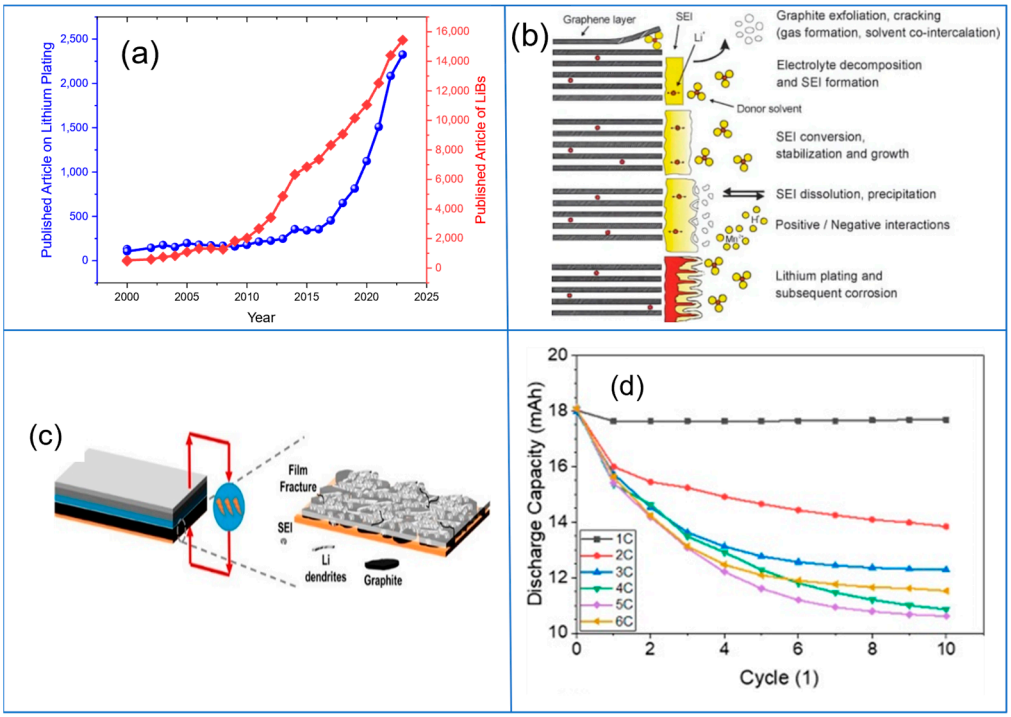

Figure 1. (**a**) Current trend in research articles on LiBs; (**b**) different degradation processes in LiBs [39]; (**c**) diagram illustrating the mechanics of anodic interfacial deterioration during ultrafast lithium-ion battery charging [33]; (**d**) discharge capacity variation during various fast charging rates [33].

There are numerous research articles on ex situ examination, post-mortem characterization, electrochemical characteristics, and modeling to understand the reason behind plating formation. Recently published review articles have also focused on experimental plating detection techniques, model-based mechanistic studies, machine learning-based data-driven analysis, and mitigation methods. Lin et al. presented a comprehensive review of plating-related research in 2020 [40]. Given the increased focus on plating phenomena due to the demands for fast charging in electrical vehicles, there is a need to review the recent developments critically. The primary goal of this work is to give a brief overview of and a detailed insight into the published literature on lithium plating since 2020. This review covers reported studies on plating conditions, and electrochemical characterization techniques, considers their future implications for battery management systems (BMS), and reports on the commercially feasible techniques for minimizing the plating. The review discusses the mechanisms underlying lithium plating and how electrochemical, thermal, and physical conditions influence these mechanisms. The electrochemical plating characterization techniques are briefly summarized with the potency of their utilization in battery management systems. Finally, this article discusses the efficacy and feasibility of the different lithium plating mitigation techniques.

2. Fundamental Mechanism Behind Lithium Deposition

Lithium plating is the term used to describe the deposition of the cyclable Li^+ ion as metallic lithium on the anode surface [21]. Purushothaman and Landau [4] postulated that when the Li^+ flux at the graphite/SEI charge transfer interface is greater than the Li^+ intercalating flux, the Li-ion starts to accumulate at the anode–electrolyte interface, resulting in localized charge polarization, as described in Figure 2a. Consequently, the local anode surface overpotential drops and becomes negative vs. Li^+/Li, as shown in Figure 2b [33]. This phenomenon is typically observed during low-temperature or fast charging (>1C) conditions, which cause lithium deposition to be thermodynamically more favorable than intercalation, resulting in a mono-electron reduction of the lithium-ion, as shown in Equation (1) [41,42]. Reduced lithium metal starts accumulating on the anode

surface, as depicted in Figure 2c. Some researchers also pitched the idea of lithium-ion saturation at the anode–electrolyte interface for plating initiation, which differs from the thermodynamic criteria, showing plating initiation at a negative anodic potential far below 0 V (local minima of anodic potential) for 6C charging, which corresponds to a saturation level of the Li-ion concentration (0.077 mol/cm^3) at the anode surface [43–45]. Sometimes deposition occurs above 0 V vs. Li/Li$^+$ due to local temperature gradients at the anode surface, which shifts the equilibrium potential for plating formation to a positive value [42,46–51].

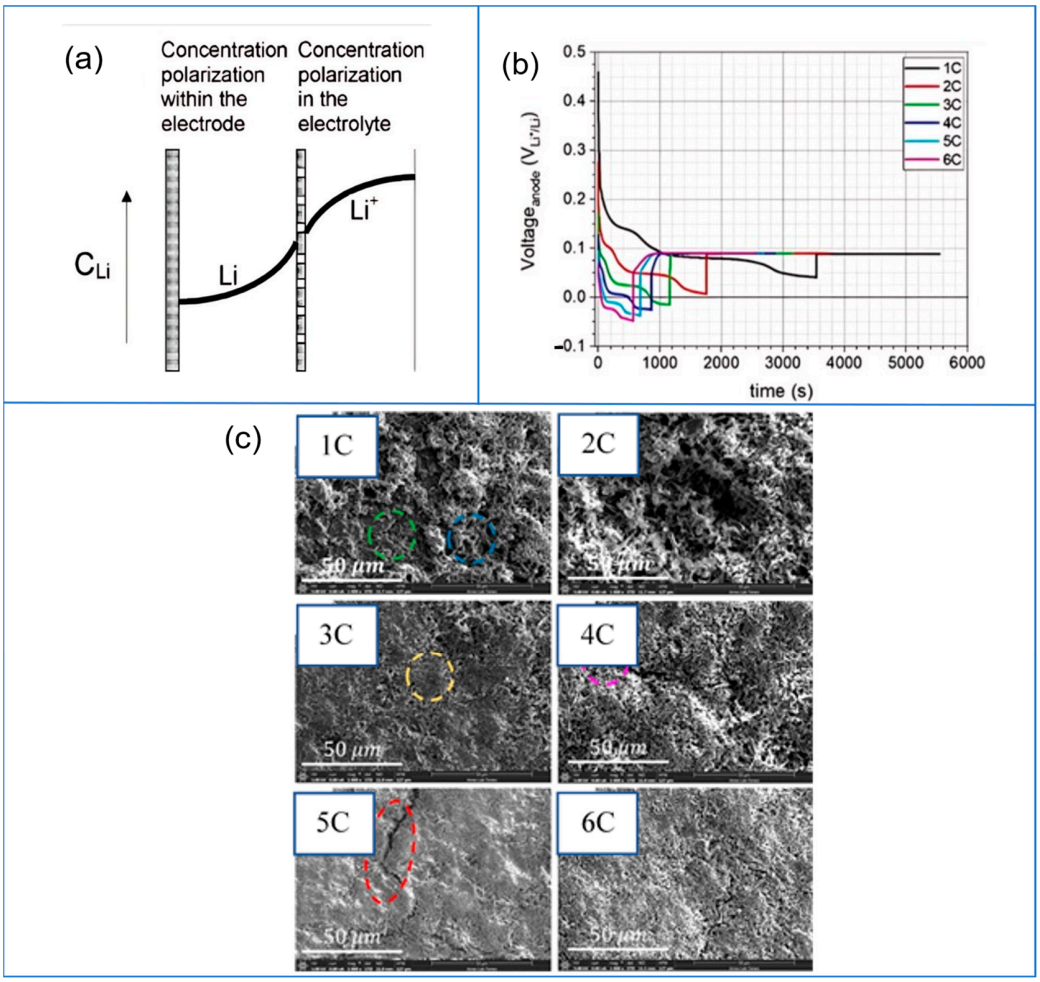

Figure 2. (**a**) Charge polarization across the electrode and electrolyte [43]; (**b**) anodic potential evolution during charging at different C rates [46]; and (**c**) anode surface evolution at 1–6C due to plating [33], coloured portion are the area where EDX scanning are performed.

The deposited lithium metal can be divided into reversible and irreversible plating. The reversible part holds an electrical contact with the anode surface. It undergoes a charge transfer reaction with the electrolyte and re-intercalates into the graphitic layer when the anode potential returns to positive ($\eta_{Li/Li^+} > 0$, vs. Li$^+$/Li). This re-intercalation, as described in Equation (2), is called lithium stripping [31,46,52–55]. In contrast, the remaining metallic portion, termed irreversible plated lithium or dead lithium, becomes isolated electrically from the anode due to the insulating SEI film covering. This entraps dead lithium in the SEI, which is seen as a whitish layer on the anode, as shown in Figure 2c (the 5C and 6C cases); it becomes unavailable for the rest of the cycling, resulting in a rapid capacity loss and a rise in the cell's internal resistance [31,33,46,56–58]. Plated material sometimes blocks the pathway for further lithium intercalation [56–58]. Irreversibly plated parts sometimes react with the electrolyte and disassociate it [31].

Plated lithium morphology depends on working conditions and charging rates. It can be segregated into three broader types. (1) The mossy form [57,59] and (2) granular particle form usually occur at a lower C rate [60]; (3) dendritic needle-type structures are observed at high C rates [58,61]. Due to its ability to puncture the separator, the dendritic structure, which results in the cell's internal short circuit following thermal runaway, is the primary safety concern among battery communities [62–68]. The studies conducted by Li et al. reported exothermic reactions between the plated lithium and electrolyte, which can also trigger thermal runaway in the cell. Still, the temperature rise is proportional to the available plated lithium [57].

$$Li^{+} + e^{-} \rightarrow Li \tag{1}$$

$$\alpha Li^{0} + \beta LiC_6 \rightarrow Li_{\alpha+\beta}C_6 \tag{2}$$

$$i_{el} = 2Fk_{el}\sqrt{c_{s,surf}\left(c_{s,max} - c_{s,surf}\right)c_e}\sinh\left(\frac{\alpha F}{\mathcal{R}T}\left(\eta - U_{OCP} - \mathbb{R}_{film}i_n\right)\right) \tag{3}$$

$$i_{pl} = \min\left(0, 2Fk_{pl}\sqrt{c_e}\sinh\left(\frac{\alpha F}{\mathcal{R}T}\left(\eta - U_{pl} - \mathbb{R}_{film}i_n\right)\right)\right); \eta < 0 \tag{4}$$

$$i_{st} = \max\left(0, 2Fk_{pl}\sqrt{c_e}\sinh\left(\frac{\alpha F}{\mathcal{R}T}\left(\eta - \mathbb{R}_{film}i_n\right)\right)\frac{m_{pl}}{\max\left(m_{pl}\right)}\right); \quad \eta > 0, \max\left(m_{pl}\right) > 0 \tag{5}$$

When plating starts to nucleate at the anode surface, the total applied charging current can be distributed into two parts: (i) lithium intercalating flux (Equation (3)) and (ii) lithium plating current (Equation (4)) [69].

During regular operation, intercalation is more thermodynamically favorable, with an anodic potential of 65–200 mV vs. Li/Li^{+}. Intercalation occurs when the overpotential of the lithium insertion is larger than the equilibrium potential of the electrode [45]. Some studies show that the kinetic factors are also responsible for plating during mild C rate or low-temperature charging [53,70,71]. Some researchers utilized thermodynamic equilibrium using the Nernst equation to understand the behavior of the plating driving force under different temperatures [72–75]. The salt concentration at the electrode surface decreases due to intercalation, but when a high C rate is applied, the incoming lithium flux exceeds the salt diffusion flux. This is comparable to the situation in the case of the dendritic deposition of other materials (such as Cu [76] and Zn [77]). This intense polarization causes the local anode potential to drop below 0 V, which might be considered a thermodynamic need for lithium plating. Conversely, the kinetics criteria, which likewise emphasize the increase in the local lithium-ion flux and assume that the graphitic anode's local interstitial site becomes saturated during intercalation, dramatically contribute to surface crowding. This ultimately forces the anode surface to receive the applied flux as metallic lithium [45,78,79]. The equilibrium potential at the anode surface has a heterogeneous distribution due to localized internal temperature change [31]. Therefore, during charging, heat generated due to joule heating may reduce the equilibrium plating potential over intercalation potential and may cause the thermodynamic favorability of the localized lithium plating [53,59,60]. It should be remembered that thermodynamics understanding also has limitations during the high C rate charging process when the assumption for the Nernst equation is not valid due to the system's dynamic nature [72,80]. However, at low temperatures (~0 °C), a reduction in the solid-state diffusion and slower kinetics causes lithium-ion accumulation at its edge plane, resulting in lithium plating [81]. Xiang et al. showed lithium plating concentration at the anode–separator interface compared to the current collector side due to large polarization [82]. Yoenguk et al. also showed that pouch cell irreversible plating loss is lower than coin cells [83].

In summary, when the incoming Li^{+} flux becomes high enough compared to the local salt diffusion or intercalation flux, it leads to lithium plating. The loss of cyclable lithium

modifies the electrode's capacity balance and reduces the incoming flux, ultimately stopping the plating process entirely during fast charging or low-temperature charging [31,33,84–88].

3. Reason for Lithium Plating

3.1. Internal and External Factors Affecting Lithium Plating

Numerous studies have determined how lithium plating happens under different circumstances. Two primary variables can influence lithium plating, as shown in Figure 3: (I) internal variables, such as (a) manufacturing condition and local defect, (b) age of the cell, and (c) heterogeneous electrolyte distribution, and (II) external variables, such as (a) operating temperature (low and non-uniform temperature gradient), (b) load application (external and internal), (c) high charging rates, and (d) overcharged condition.

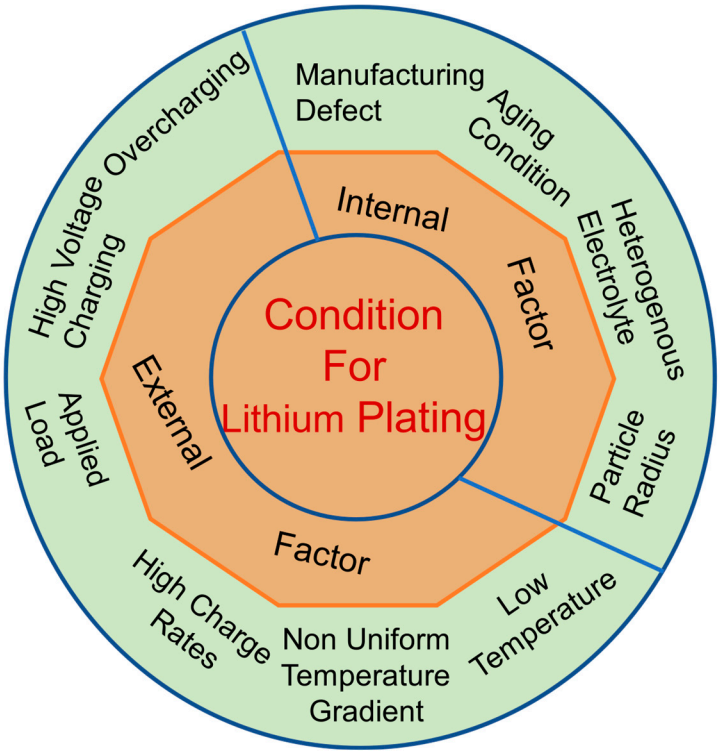

Figure 3. Different external and internal factors affecting lithium plating.

3.2. Internal Variables

3.2.1. Manufacturing Conditions and Local Defects

Electrode surface, particle radius, porosity, interparticle connection, and separator quality play a vital role in the nucleation of lithium plating. Lithium plating occurs due to internal defects, such as deformation in the separator, uneven anode surface, and internal mechanical stress [32,80,89]. Non-uniformity of the separator due to manufacturing defects and external pressure clogging the separator pore may create uneven localized flux, which impacts the local electrochemical activity and eventually catalyzes the lithium plating [15,90–92]. This localized deformation due to the cell's regional architecture initiates plating near the edge of the cell, as shown in Figure 4a [59,91–94]. Elevated anode thickness and increased defects on the basal plane also impede the mobility of lithium ions in the basal plane. Retarding the diffusional motion at the edge plane increases the susceptibility to lithium plating [95]. Hence, the surface structure of the graphite anode also plays a critical role in the plating mechanism. It also accelerates the dendritic lithium deposition.

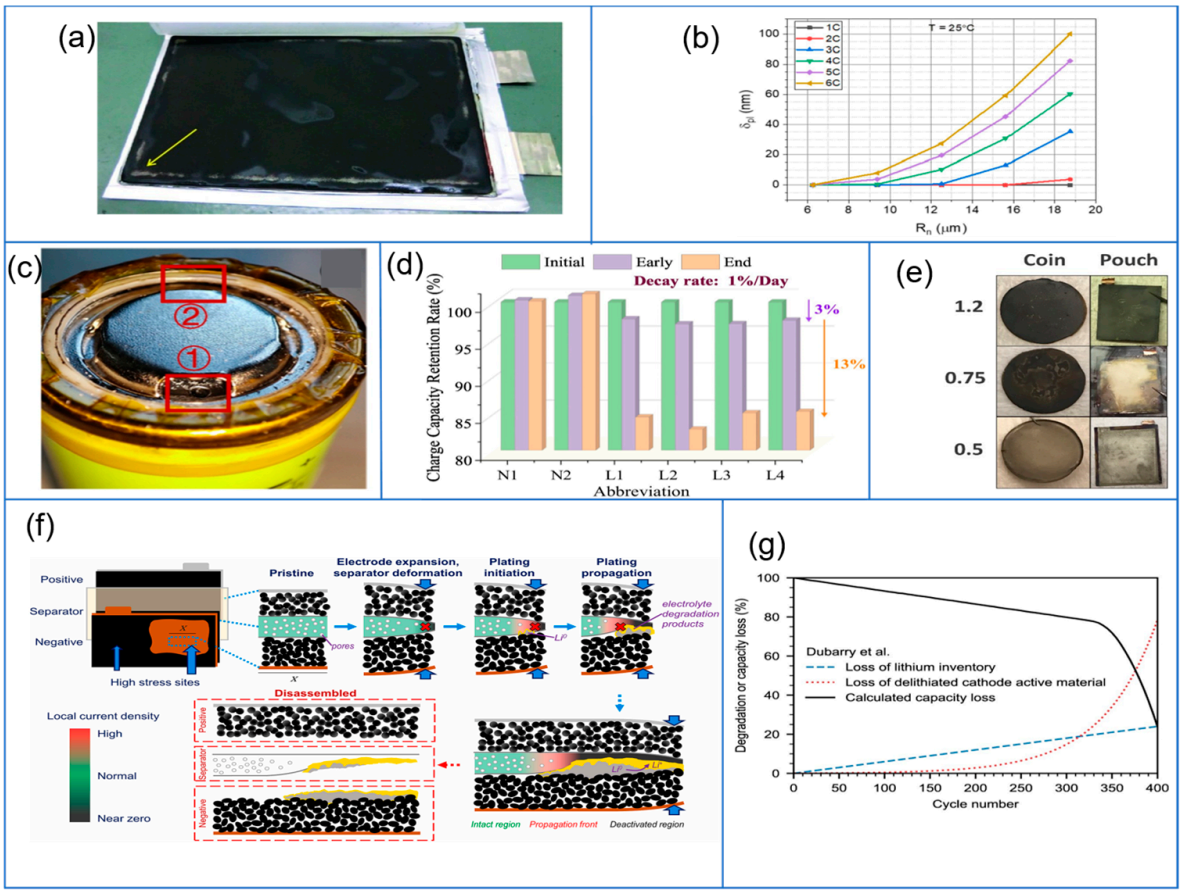

Figure 4. (**a**) Lithium plating nucleation near the edge of the cell [59]; (**b**) effect of particle radius on plating at different C rates [69]; (**c**) localized electrolyte leakage (Drilled locations for electrolyte removal are marked with red rectangles and serial no) [85]; (**d**) capacity lost due to unavailability of electrolyte [85]; (**e**) change in plating tendency due to different mass (N/P) loading [86]; (**f**) probable plating initiation condition under mild C rate cycling. The figure highlights that localized electrode and separator deformation initiates plating nucleation (The Red cross marks separator deformation zone) [87]; (**g**) knee-shaped rapid drop in recyclable capacity after long cycling due to the plating [88].

McShane et al. and Tang et al. provide evidence of the geometrical effects on the plating phenomena. Tang et al. also developed a correlation between the overpotential distribution for anode sizes and the electrolyte contact area across the cell [96,97]. Sarkar et al. used physics-based modeling to show an exponential rise in plating severity with the anode particle radius (Figure 4b) [69]. Wang and his co-author also reported a proportional surge in localized plating in cylindrical cells due to electrolyte drying out or leakage, as shown in Figure 4c,d. They found that localized drying out of electrolytes increases the surrounding Li^+ flux, making a favorable condition for lithium plating [85]. Yang et al. highlighted that the planar diffusion of electrolytes on the graphite electrode sometimes becomes very limited due to external pressure or flawed packing. This limited the Li^+ migration and distribution results in the inhomogeneous Li^+ flux and subsequent polarization and lithium plating. This phenomenon was also observed in the case of pouch cells, where a higher amount of plating was observed near the tip compared to the central portion [98].

3.2.2. Aging Condition

Previously, people used to think of plating as a fast or low-temperature charging phenomenon. However, with time, the researcher found many conditions, described in Table 2, which can initiate lithium plating. Peter et al. reported the observation of plating phenomena at a mild C rate after long cycling. During long cycling, the plating initiation

occurs due to the delamination of anodic active electrode material, which increases localized effective lithium-ion flux [88]. Deichmann et al. experimentally showcased the initiation of lithium plating when the negative to positive electrode mass (N/P) ratio falls below 1, as shown in Figure 4e [86]. Dubarry et al. also demonstrated plating nucleation following a rapid knee-shaped drop in the capacity, as described in Figure 4f, when the negative electrodes become saturated due to a decline in the sufficient anodic capacity beneath the positive electrodes at a later cycling stage. This anodic capacity loss was related to delamination, and the resistance increased, resulting in localized heterogeneity of the Li^+ flux [99]. Smith et al. described the close interrelationship between the deactivation of the anode and separator area with the nucleation of lithium plating [87]. Zhou et al. also showed deep discharge cycling that negatively impacted the intercalation site, making the anode vulnerable to lithium plating [90]. Separator deformation can also occur due to local internal mechanical stress buildup during cyclical electrode expansion [87] and internal gas evolution [92]. Separator deformation or electrolyte degradation has also caused a localized increase in flux, which initiated lithium plating commencement under mild C rate cycling, as evidenced by the knee-shaped decline in discharge capacity in Figure 4f [88].

Table 2. Different external/internal conditions affecting lithium plating.

Plating Condition Type	Description	Causes and Condition	Ref
Internal	Manufacturing and Shape Defect	Localized separator defects due to inconsistent manufacturing or non-uniform electrolyte distribution create current non-uniformity, significantly influencing plating.	[15,85,90,91,96–98]
Internal	Aging	Aging drives the delamination of anodic material and the corresponding reduction in active surface area and resulting lithium plating.	[86–88,99]
External	High CC-CV Charging Rates	Fast charging generates large lithium-ion flux toward the anode, but the anode solid intercalation remains slower. This leads to lithium-ion accumulation at the particle surface.	[46,69,89,100–102]
External	Operating Temperature	Low temperature reduces electrode diffusivity and induces slower kinetics, generating charge polarization at the anode–electrolyte interface.	[31,43,86,101]
External	Overcharging	Overcharging the cell around 4.5 V forces more lithium into the anode, causing accumulation at the anodic interface.	[31,63,89,103]
External/Internal	Load	Pressure clogs the separator pore, increasing localized current flux and resulting in lithium plating. In contrast, limited external pressure causes stable plating growth.	[90,91,104]

3.3. External Variable

3.3.1. Effect of High Charging Rate Protocol

Fast charging is becoming increasingly popular across industries, from electric vehicles to electronics. However, rapid lithium plating, resulting in a capacity drop, as shown in Figure 1d, is the main roadblock for fast charging utilization. The higher lithium-ion intercalation flux during fast charging creates charged ion polarization near the anode, and the following drop-in anodic potential makes the lithium plating favorable compared to intercalation, as described in Figure 2b [46,69,89,101]. Sarkar et al. showcased rapid capacity loss with C rates due to plating, as shown in Figure 2c [33,69]. Wang et al. also experimentally quantified the graphite anode limitation that causes polarization in the electrolyte during fast charging. Their work showed that the cathode also significantly contributes to electrolyte polarization [102].

3.3.2. Operating Temperature

Low Temperature

Plating phenomena under low-temperature charging are widely known. Lithium-ion battery performance will be substantially diminished in cold temperatures, as shown in Figure 5a, because of the increased cell impedance and reduced kinetics behavior [60]. Jaguemont and his co-author showed that lithium-ion battery capacity dropped by 39% at −20 °C compared to 25 °C. At low temperatures, slower lithium-ion diffusion at the anode–electrolyte interface and slower intercalation cause Li^+ accumulation, resulting in rapid lithium plating [105]. Cho et al., using impedance analysis, discovered that a reduction in charge transfer resistance is the leading cause of cell polarization from −5 °C to 25 °C [106]. Hence, mass transfer limitation due to slower diffusion and limited kinetics results in a drop in the potential of the anode to below 0 V vs. Li/Li^+, causing Li^+-ion reduction and a rapid drop in the available capacity of the cell, as shown in Figure 4c–e [21,31,64,85].

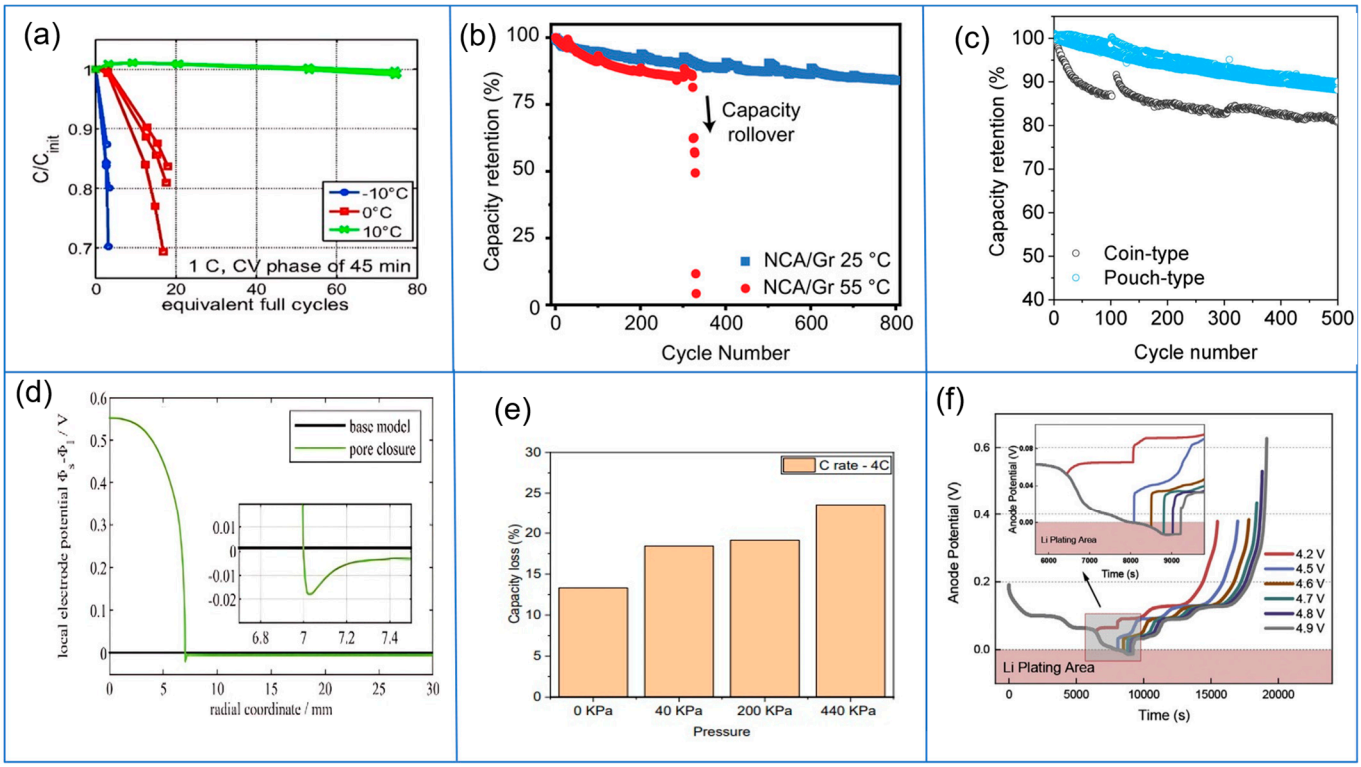

Figure 5. (**a**) Remaining normalized capacity vs. equivalent complete cycles number for cells charged under a range of temperatures at 1C rate [89]; (**b**) cyclic capacity retention of NCA/C cell at room and elevated temperature at 0.5C rates [27]; (**c**) cycling performance between coin cell and pouch cell [83]; (**d**) dropping of anodic potential due to pore closure [84]; (**e**) capacity loss (%) vs. externally applied pressure at fast charging rates [54]; (**f**) considerable drop in anodic potential during overcharging conditions at C rate [103].

Non-Uniform Temperature Gradient

Generally, lithium plating is not observed during a high-temperature operation. Conversely, Wang et al. reported an increase in the plating tendency for a 10° rise in temperature on the graphite electrode because of shifting the plating equilibrium potential to positive voltage, which made plating initiation more thermodynamically favorable than intercalation. Thermodynamic plating criteria differ from kinetic limitation at low temperatures and are responsible for rollover failure under high-temperature mild C rate charging, as shown in Figure 5b [27]. Dr. Carter's work also showed a similar plating observation due to the inter-electrode temperature gradient. They showed the existence of lithium plating around 35 °C due to a 2° inter-electrode temperature difference when the cathode temperature

was on the higher side [107]. On the other hand, Jialong et al. and Guangxu et al. also described the reaction of plated lithium with electrolyte at high temperatures, which generated gas and caused the cell to swell up and increased the charge transfer resistance [26,108]. Yuan et al. also reported a thermal runaway due to the irreversibly plated material reaction with electrolytes during high-temperature cycle aging [26,101,109]. Regarding the safety of the battery operation, electrolyte decomposition and swelling up, followed by thermal runaway, are the primary concerns [110].

3.3.3. Effect of Applied Loads

There is continuous progress toward understanding the effect of pressure on plating because the cells are stacked on top of each other in the battery pack. The mechanical pressure on the cell stack in the battery pack and the encasing with the internal spring in the coin cell also create localized stress and the deformation of the anode and separator. Most batteries are sealed at vacuum pressure, around 50 mBar. Hence, air pressure also adds up on the cells. In the case of cylindrical cells, the outer casing is stiffer than the inner circumference, causing uneven pressure distribution across the cell. High compressive stress also shows increased overpotential and cell impedance at the anode suitable for the plating initiation. This accelerates capacity decay in the coin cell case, as shown in Figure 5c [83,111].

Peabody et al. showed that externally applied compressive loading caused localization of the lithium plating due to separator pore closure near the load's application point [90,91]. Pan et al. reported on the relationship between a drop in separator porosity and an externally applied load [93]. Spingler et al. reported that localized compressive loads up to 10 MPa were responsible for separator pore closure, resulting in a negative anodic potential near the separator at the end of CC charging, as shown in Figure 5d [84]. Gargh et al. demonstrated that external pressure on the pouch cell during fast charging caused excessive irreversible lithium plating, which can be seen (Figure 5e) as the rise in the capacity loss with the externally applied pressure [54]. However, Lee et al. and Fang et al. demonstrated that uniform stack pressure up to a specific limit could cause stable plating growth and inhibit dendritic growth, ultimately reducing irreversible plating losses and improving coulombic efficiency and cell life [112,113]. Cao. et al. also demonstrated a homogenous plating reaction across the cell (vertically and laterally) due to external pressure during fast charging [114]. Robert's research group described the effect of pressure in two stages; during the initial to moderate stage, the applied pressure induces stress, suppressing the dendritic of the metallic lithium on the anode. When it reaches a threshold limit, the pressure starts to close the pore of the separator, causing non-homogenous localized lithium deposition [68]. Hence, localized load application plays a critical role in the battery performance.

3.3.4. Overcharging and High State of Charge Condition

Different reports have been published on lithium plating under overcharged conditions. Overcharging of the graphite anode shows a significant drop in the anodic electrode potential to the negative region during charging, resulting in lithium plating, even at a smaller C rate [31,63]. Madeleine et al. showed heavy, denser plating layer deposition near the separator during charging up to a high state of charge [89]. Researchers also showed that plating is observable under high-voltage conditions, around 4.5–4.586 V, even at a lower C rate. Figure 5f shows a more significant drop in anodic potential due to overcharging of the cell. Furthermore, they found a linear correlation between the lithium plating initiation time and the capacity with an overcharge voltage at 0.2C and 0.5C [103].

4. Plating Characterization and Estimation

For the last two decades, numerous research works have been conducted to detect lithium plating [20,40,115,116]. These characteristic techniques are classified as destructive and non-destructive. The well-developed destructive characterization techniques are visual microscopy [117], scanning electron microscopy and energy dispersive X-ray spectroscopy [33], X-ray photoelectron spectroscopy (XPS) [33], nuclear magnetic resonance spectroscopy (NMR) 50], neutron diffraction [118], electron paramagnetic resonance (EPR) [33,69,119], atomic force microscopy (AFM) [61], transmission electron microscopy (TEM) [108,120], Fourier transform infrared spectroscopy (FTIR) [121], and inductively coupled plasma optical emission spectrometry (ICP-OES) [122]. In comparison, the non-destructive characterization methods, as described in Table 3, include electrochemical impedance spectroscopy (EIS) [57,123–127], voltage relaxation plateau analysis [33,46,68,128–130], reference third electrode (RE) [102], dynamic capacity measurement [131,132], incremental capacity and differential voltage curve [31,55,133], coulombic efficiency (CE) and discharge capacity [33,134,135], and physics-based electrochemical model prediction [46,136–142]. This article primarily focuses on the recent development work on electrochemical-based non-destructive electrochemical plating characterization techniques that can be applied at the whole cell level and are a potential candidate for future application in battery management systems (BMS) during cycling.

4.1. Electrochemical Impedance Spectroscopy (EIS)

Electrochemical impedance-based sensing is a popular method to obtain an insight into the electrochemical processes inside a lithium-ion cell. During EIS, AC pulses are employed to separate the different electrochemical reactions based on the time constant of each reaction step. The EIS data represented by the Bode plot show the cell's total impedance (left axis in Figure 6a) and the corresponding electrochemical phase change (right axis in Figure 6a). At the end of fast charging during the voltage relaxation, a continuous EIS scan provided a detailed insight into the impedance evolution because of the intercalation of metallic lithium due to stripping. It caused the rise of the overall impedance of the cell due to the decreased higher conductivity of the plated material, as shown in Figure 6b. At the 1C charging rate, shown in Figure 6a, no impedance evolution occurred due to a negligible amount of plating. In contrast, impedance change occurred at 3C due to the higher presence of plated material [57]. The distribution of relaxation times (DRT) analysis has also been employed to de-convoluted time-dependent impedance observation of different electrochemical reactions inside the batteries. The spectrum shows a rising anodic interface resistance during the relaxation period after charging (Figure 6c). During the relaxation period after fast charging, stripping occurs, causing the rise of the anodic film resistance [57,127]. Researchers sometimes used the equivalent RC circuit model by comparing experimental and model-predicted EIS spectra to extract information about different electrochemical mechanisms [57,131].

Some of the BMS systems that are currently available frequently monitor the battery's internal impedance using the EIS plot's low-frequency turning point to detect lithium plating [123]. Researchers also showed that EIS, an in-situ method, can quantify the degradation, such as lithium inventory loss, conductivity loss, and active material loss [124,125]. Figure 6d schematically shows the result of a dynamic EIS scan during plating nucleation through a drop-in charge transfer resistance in the Nyquist plots. EIS measurement is sensitive to the instrument, temperature, state of charge (SOC) of the cells, and applied AC amplitude [126]. The EIS signal is limited to a qualitative understanding of lithium plating. Although it can be used as an online detection method, it has specific requirements for specialized instruments, which are costly, bulky, and less suitable for adoption in automobile applications.

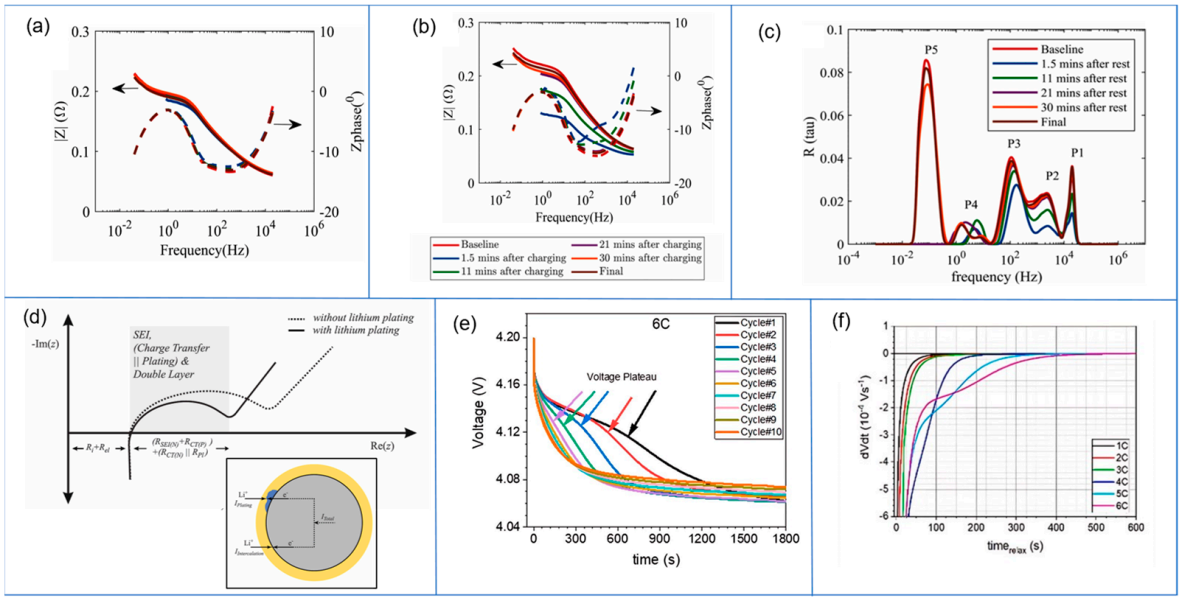

Figure 6. Bode figure showing the pouch cell battery's impedance evolution during voltage relaxation immediately following fast charging for EIS scans carried out at charging rates of (**a**) 1C and (**b**) 3C; (**c**) distribution of relaxation times (DRT) spectra during relaxation voltage after 4C fast charging rate [57]; (**d**) a generic change in Nyquist plots due to plating [126]; (**e**) voltage plateau analysis during 6c fast charging [33]; (**f**) relaxation open circuit voltage gradient vs. time plot for different charging rates during the relaxation period [46].

4.2. Voltage Plateau Analysis (VRP)

Voltage plateau analysis, another common approach, is used to detect the signature of the lithium plating. It measures the cell terminal potential change to detect the plating. After the end of charging, the anode potential rises, and when the anode voltage becomes positive, reversible plated lithium starts to intercalate into the anode [68,128]. The energy change during this transformation is reflected as a voltage plateau (Figure 6e) and also by measuring the slope (dV/dt) change of the open circuit voltage (Figure 6f) [33,46,129]. Figure 6e shows the shift of the plateau to a lower time due to the suspension of plating during the later stage of fast-charge cycling [33,46]. VRP also computes stripping completion time using the location of the dV/dt maxima peak. The dV/dt peak size can be easily correlated with reversible plated lithium mass; Figure 6f shows an increase in peak height and stripping completion time at higher C rates [130]. Conversely, some researchers found that voltage plateau is the total contribution of phase changes due to stripping and concentration equalization in the lithiated graphite phase [52]. VRP does not explicitly quantify the capacity of the reversible plating phase, and it also does not detect stripping when the reversible plated mass is significantly low [52,125,135].

Table 3. Different types of electrochemical characterization and estimation techniques.

Characterization Types	Ex Situ	In Situ	Advantages	Disadvantages	Ref
Electrochemical Impedance Spectroscopy		X	It can detect and quantify the trend of degradation mechanisms.	It required a controlled and stable electrochemical system with specialized equipment.	[57,114–117,123]

Table 3. *Cont.*

Characterization Types	Ex Situ	In Situ	Advantages	Disadvantages	Ref
Voltage Plateau (VRP) Analysis		X	VRP detects phase change in reversible lithium during stripping.	It cannot quantify the actual plating and stripping capacity.	[33,46,68,128–130]
Incremental Capacity (IC) and Differential Voltage (DV) Curve		X	IC and DV can detect the stripping lithium and its mass during discharging.	It does not provide information on the total plating loss and the stripping mass during CV charging.	[31,55,133]
Coulombic Efficiency (CE) and Discharge Capacity		X	Most of the battery testers collect these data as a primary measurement. A significant drop in it signifies lithium plating.	It does not differentiate between different losses and fails to quantify them individually.	[33,134,135]
Dynamic Capacity Measurement		X	DCM can dynamically indicate the onset of lithium plating and stripping in real time. It can also monitor the change in the capacitance of the electrical double layer.	DCM requires a specific frequency. Otherwise, its measured reading will be noisy and overlap with the cathodic background signature.	[131,132]
Physics-based and Data-driven Modeling		X	Physics-based electrochemical modeling provides insights such as plating onset time, degradation quantification, and its behavior under different conditions.	It requires specialized domain knowledge and higher computing power.	[46,136–142]

4.3. Incremental Capacity and Differential Voltage Curve

Incremental capacity (IC) and differential voltage (DV) curve analysis are crucial in situ measurement methods to detect variations in the cell's electrochemical characteristics. These methods assume equilibrium states of the cell when discharging is conducted at shallow currents around C/25 to C/10. They measure the charge Q and the pseudo-OCV (pOCV) across the terminal. Differential or incremental capacity (dQ/dV) refers to a change in cell capacity (dQ) due to a unit change in voltage (dV). This is plotted as (dQ/dV) vs. voltage, as shown in Figure 7a [26]. The drop in peak height and the shift of peak voltage usually results from SEI formation, plating loss, particle breaking, and delamination of active material [133]. The high-voltage plateau in differential capacity plots is related to reversible plated lithium (during stripping). This high-voltage plateau shrinks and sometimes vanishes as the cycle count increases, indicating plating suspension. A small peak shift also occurs due to increased cell impedance [31]. The high-voltage DC peak is shifted to a higher voltage side during charging and vice versa during discharging due to the deposition of irreversible plating material, which is responsible for the rise in the cell's overall impedance and retards the lithium-ion movement at the interphase [55].

On the other hand, differential voltage analysis (dV) refers to a change in voltage for a unit change in capacity (dQ). This is plotted as dV/dQ vs. Q (capacity), as shown in Figure 7b [31]. The observed peaks are formed due to the several stages of the intercalation process. The different peaks provide significant evidence of the multiple-phase transition of lithium carbon compounds inside electrodes during cycling [133]. The plateau in the high voltage zone signifies the capacity loss due to plating. The shrinkage of the differential voltage plots indicates a lower availability of cyclable lithium. Low-capacity peaks in dV plots have also been used to detect the reversible capacity of plated lithium during stripping [115]. This technique can be used as a post-processing tool, but it lacks real-time application.

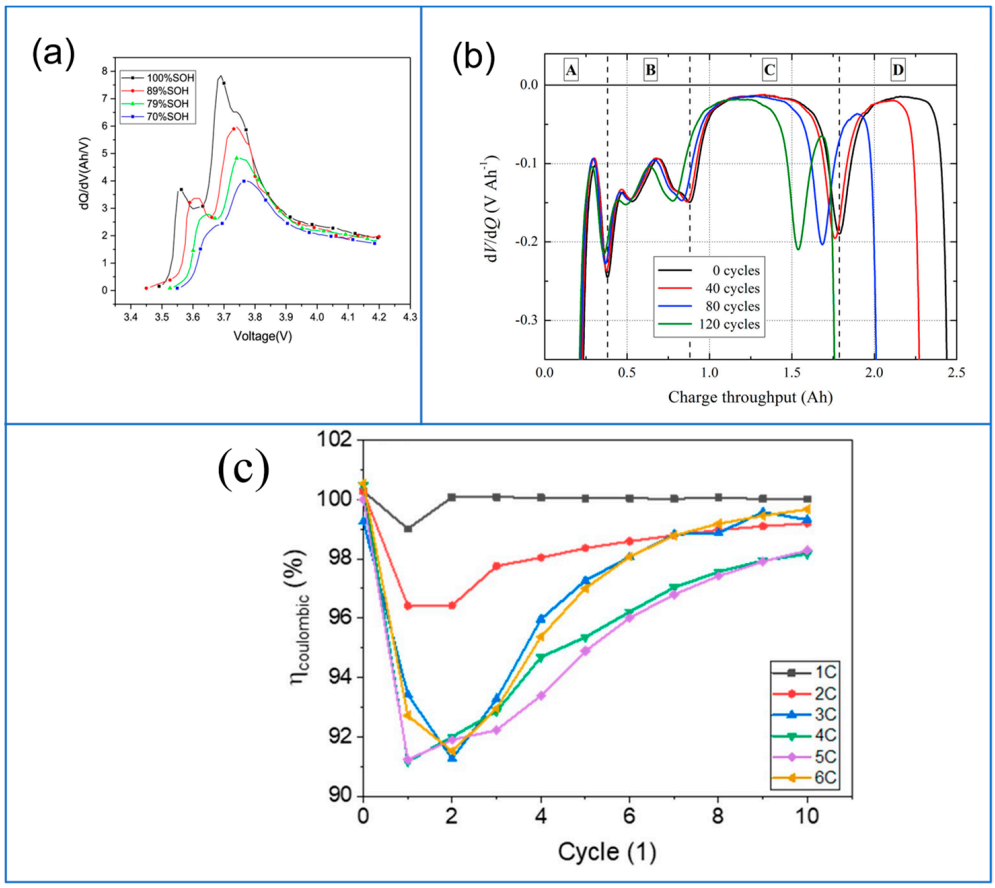

Figure 7. (**a**) Incremental capacity curves at different SOH from the capacity test [26]; (**b**) differential voltage plots during low-temperature cycling due to LLI loss (A–D refers to different stages of phase change within cathode/anodes during lithium deintercalation/intercalation) [31]; (**c**) coulombic efficiency variation during fast charging [33].

4.4. Discharge Capacity and Coulombic Efficiency (CE)

Discharge capacity is a measure of available recoverable capacity during discharging. Typically, the loss in discharge capacity is prolonged due to SEI growth, but when plating happens, the irreversible part causes a rapid drop, as shown in Figure 1d [33]. On the other hand, the ratio of the energy (Qd) that a LiB releases during discharge to the energy (Qc) that a LiB absorbs during charging is known as the coulombic efficiency (CE). After plating, some plated lithium is not available for stripping [134]. Due to this cyclable lithium loss, coulombic efficiency falls drastically, as shown in Figure 7c. This rapid decrease in coulombic efficiency during fast or low-temperature charging and rapid discharge capacity loss are primary indicators of the plating deposition on the graphite anode [33,135].

4.5. Dynamic Capacity Measurement and Differential Current Analysis

With the development of sensing technology, the plating initiation can also be observed during charging. Single-frequency dynamic EIS, also known as DCM, was used by Xu et al. to monitor the change in electrochemical active surface area (ECSA) and the electrical double layer (EDL) capacitance to detect the onset of lithium plating using the change in capacitance, as shown in Figure 8a. The increase in the capacitance of the EDL on the anode surface is used as a quantitative indicator for Li plating. They reported that the characteristic frequency of the graphite anode's charge transfer mechanism was 15.0 Hz; it was used to monitor the dynamic capacitance variation on the graphite anode. The ECSA linearly rises with the initiation of Li plating [131]. Koseoglou et al. observed a fluctuation in the magnitude of the charging current during plating initiation using differential current

analysis (dI/dt). They found that the decaying constant voltage (CV) current suddenly became constant during lithium plating and increased during stripping. This change in the slope of the terminal current can be analyzed with differential current-to-capacity or time analysis, as shown in Figure 8b. They combined the equivalent circuit method with the charging current study as a qualitative tool to understand the onset of plating deposition during CV charging. The current fluctuation can be related to the plating onset following the stripping of plated material during charging [132].

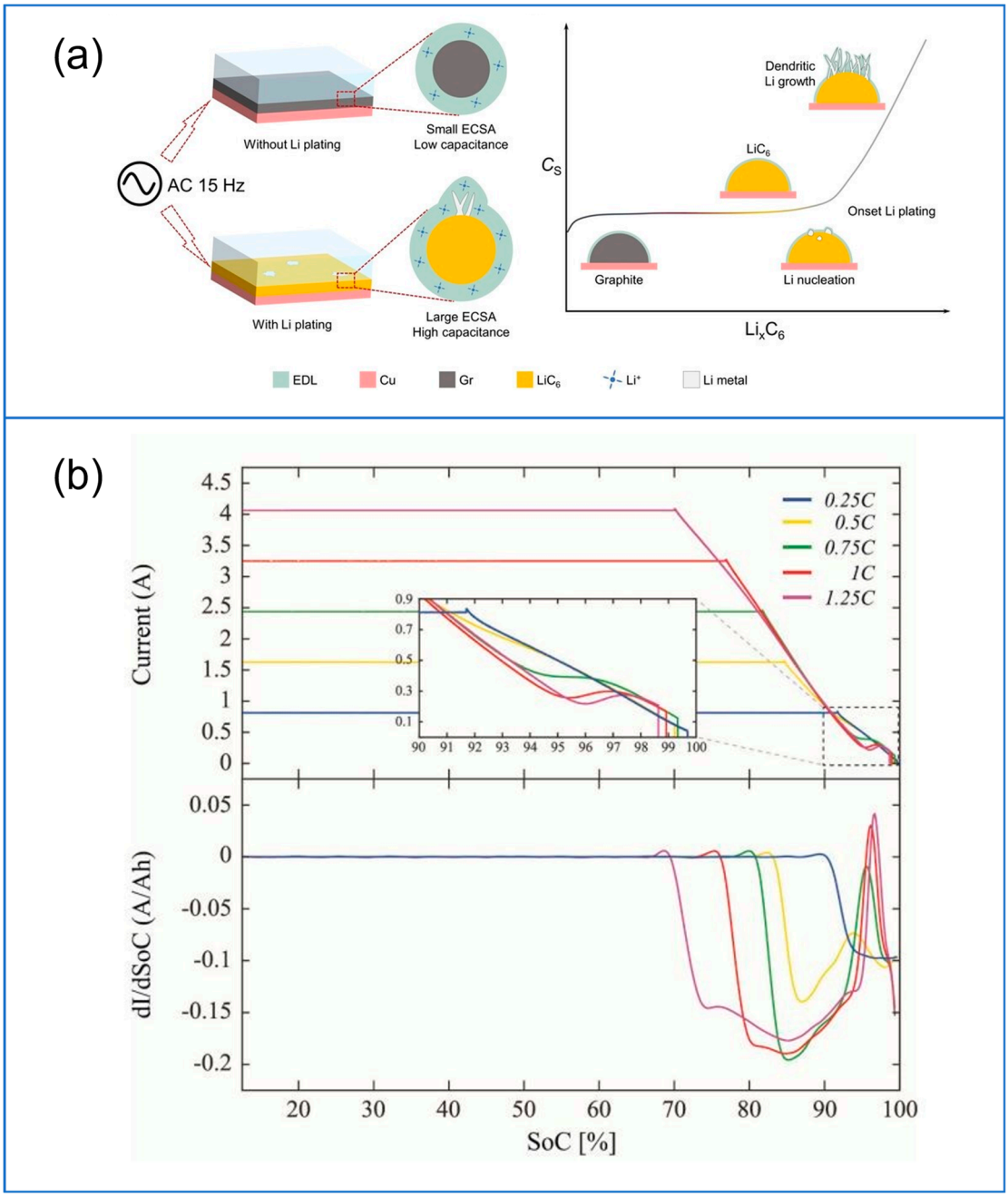

Figure 8. (**a**) Using single-frequency dynamic capacitance measurement (DCM); capacitance at the negative electrode due to increased localized surface area when plating deposition occurs [131]. (**b**) Variation in the slope of the terminal current during CCCV charging due to plating [132].

4.6. Physics-Based and Data-Driven Modeling

Physics-based numerical models are great tools for understanding a chemo-physical system's internal dynamics. These are used to study interaction mechanisms in lithium-ion batteries. These models are used as a forecasting and analytical tool to analyze plating degradation in LiBs. They also estimate cycle life, capacity loss, and suitable conditions to minimize the batteries' plating degradation. The pseudo-2D model (1993) proposed by Doyle–Fuller–Newman and the reduced-order SPM model are commonly used to study lithium batteries [136,137]. A physics-based model can predict the Li deposition's onset time for a particular charging condition. It can also correlate the Li deposition's tendency towards ionic localization and current density at the electrode–electrolyte interface [138]. Yang et al. [143] and Sarkar et al. [69] incorporate the plating mechanism in a single particle model as a reversible Butler–Volmer kinetics mechanism, as shown in Equation (4), correlating concentration-based overpotential and interface kinetics. In the single-particle model, the electrode was considered a single particle with linearized current distribution across the electrode, as shown in Figure 9. They also introduced a stripping mechanism as a function of plating volume, as shown in Equation (5). Their model distinguishes the contribution of the different electrochemical kinetics during fast charging [46].

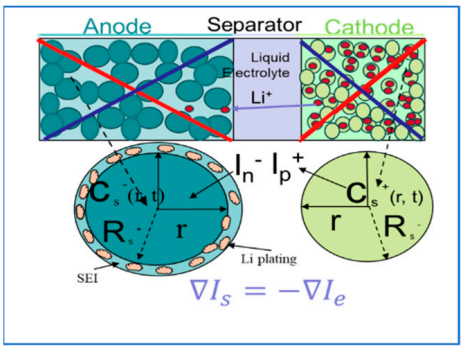

Figure 9. Single-particle model for LiBs with linearized current distribution. (The red line signifies electrode current, blue line refers to electrolytic current).

Duan et al. also focus on a similar modeling strategy for the plating. However, they model the lithium stripping as a function of lithium concentration in electrolyte and anode material. Their model can effectively capture the onset time for lithium plating, which will help to design a charging strategy for lithium-ion batteries [144]. Latz et al. proposed a physics-informed model that correlated well between the affected parameters, such as anode overpotential and cell overall potential, with the onset of lithium plating at different temperatures. They also reported a simpler equivalent circuit model using the interrelationship between anodic overpotential and cell voltage [145]. Equivalent circuit modeling focuses primarily on current distribution analyses with RC (resistance-capacitor) equivalent circuit-based models. These models have limitations in establishing a relationship between the electrochemical processes with physical parameters [80,84,138]. Zhao et al. incorporated a thermal runway into the plating model to study the gas generation due to the reaction of plated material with the electrolyte [110]. It demonstrated the effect of plating and SEI growth with thermal heat generation. Gao et al. also reported a coupled electrothermal model with a heat temperature impact to study the heat generation during battery cycling. They focused on the early plating formation and its severity during low-temperature operation [139,140]. Liang et al. also examined the electrode particle size effects on plating degradation using a similar P2D model [141]. Mukul et al. reported on another type of macro-scale model with a porous electrode system that can capture plated lithium concentration at the tip of the cell [142]. Physics-based models are good in terms of accuracy, but they are computationally extensive. To close the gap, the data-driven model has also been developed. However, the data-driven model has limited use due to its accuracy.

Conversely, there is an increase in reported literature on data-driven-based battery modeling. They utilized battery-generated data to predict the performance of LiBs. These models only work within their data range and fail significantly outside their domain. Researchers have also devised a solution incorporating physics-based information in a data-driven model. Dufek et al. used physics-based signatures, such as drop-in coulombic efficiency, anodic potential, differential capacity, and voltage plateau, after charging to develop a machine-learning algorithm to detect plating from an extensive training set [146]. In addition to this, Weddle et al. also reported another constructive approach to creating a deep learning-based battery health estimation model by incorporating estimation from physics-based information related to measured LLI and LAM loss. Their developed model showcases a higher range of efficacy for battery health prediction during rapid charging [147].

5. Mitigation and Countermeasures

Scientists worldwide are working to counter and mitigate the plating tendencies of lithium-ion batteries. Since the last decade, reports have emerged on methods that can be incorporated at the cell level to minimize the plating. Reviews have been conducted that summarize those measures in the previous decade [40]. However, more comprehensive reviews about commercially feasible technology for plating mitigation are still needed. This part summarizes all the methods, as described in Table 4, reported in this decade to reduce the plating tendency of all lithium-ion cells.

5.1. Electrolyte Engineering

5.1.1. Solvation Behavior Modification

Lithium deposition occurs due to the slower kinetics at the anode–electrolyte interface, a rate-limiting step during fast or low-temperature charging [148]. The study by Persson et al. showed that diffusion limitation caused by the slower Li^+ desolvation process and slower kinetics makes a favorable condition for lithium plating [149]. Their work showed an accelerated desolvation process by adding weakly solvating solvents or highly concentrated electrolytes, eventually lowering the binding energy. This eventually enhanced the low-temperature performance of the batteries [150,151]. Lei et al. reported that a weakly solvated electrolyte, including super-concentrated liquids, such as LiFSI, acetonitrile, and Fluorobenzene, accelerates the Li^+ desolvation process, as depicted in Figure 10a. This method showcased a 91.1% capacity retention over 200 cycles during a -40 °C temperature operation [148]. However, the mass acceptance of LiFSI is pretty limited due to its tendency to corrode the current collector. Further research is needed in this direction, and investigation is also necessary to understand the behavior of this electrolyte under different extreme conditions.

Gao et al. used an M9F1 carboxylate-ester-based electrolyte system, which showed a capacity retention of 82.5% at a 4C rate over 1000 cycles, compared to a 73.2% retention for the Gen 2 electrolyte. The M9F1 system provides quick, targeted lithium-ion transport and facile desolvation to reduce the liquid phase polarization during high-rate charging [152].

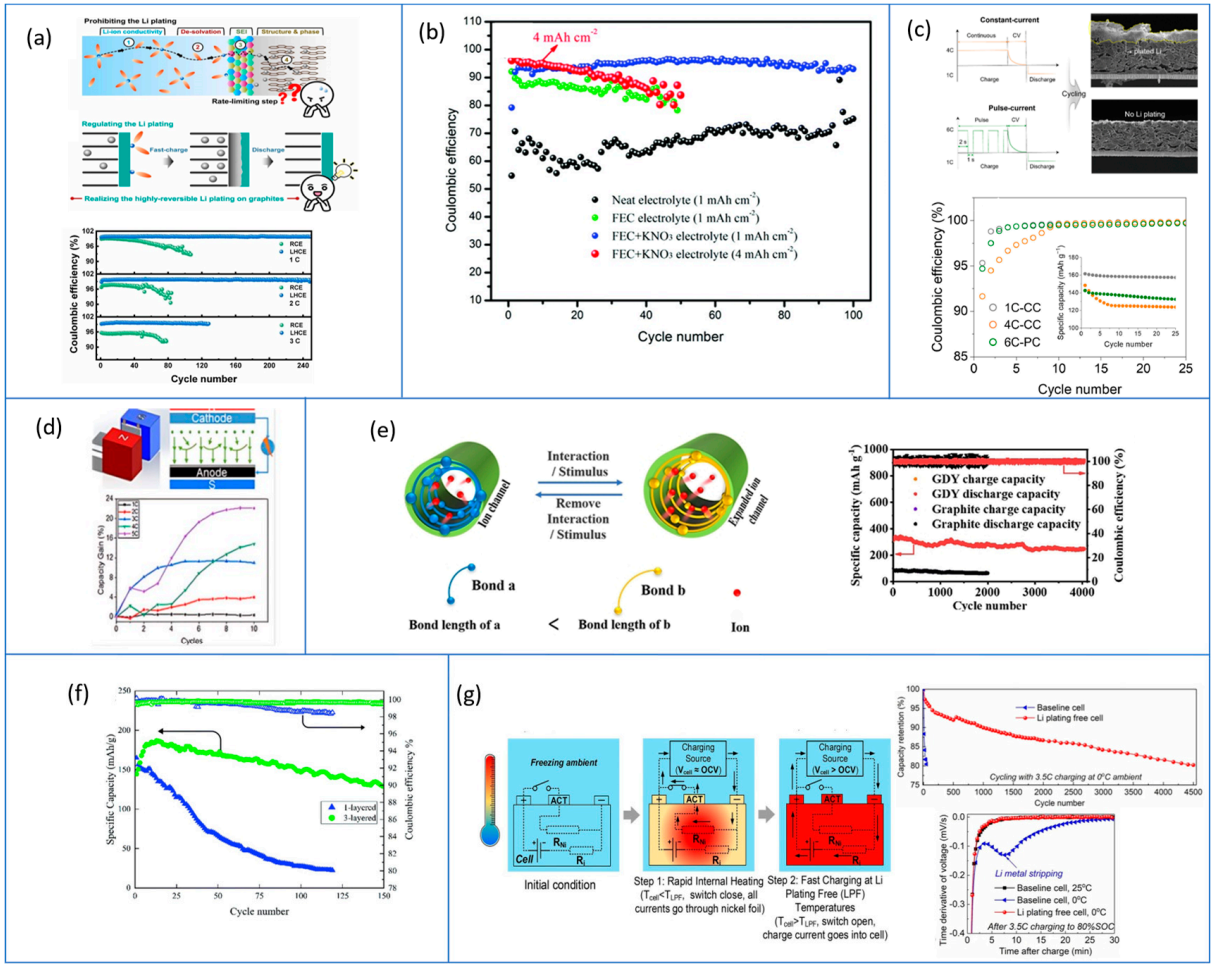

Figure 10. (**a**) Schematic diagram of the solvation process and following intercalation into the graphite anodes and lithium plating during fast charging [153]; (**b**) coulombic efficiency of Li||Cu electrochemical cells with different additive additions [154]; (**c**) higher coulombic efficiency due to PC charging than CC charging [155]; (**d**) capacity retention in the presence of magnetic field [125]; (**e**) diagram illustrating the self-expanding charge ion transport channels made possible by the chemical bonds' reversible transition between differing lengths and the corresponding increase in discharge capacity [156]; (**f**) increase in fast charging capacity retention due to 3 different porous layers across the anode [157]; (**g**) internal heating using external heating element before fast charging [42].

5.1.2. Additive Addition

Tris(trimethylsilyl) phosphite (TMSP) is a multifunctional additive that improves the cell's overall chemical stability and forms a stable hybrid solid electrolyte layer on the anode [158]. This multifunctional electrolyte additive (fluoroethylene carbonate and potassium nitrate) forms a self-healing electrostatic shield that can suppress the lithium dendrites at the anode. A spontaneous reaction occurs between this multifunctional electrolyte additive (FEC and KNO_3) and lithium metal, generating a stable electrostatic barrier using the K^+ ions. This eventually improves the battery performance, reflecting the high coulombic efficiency shown in Figure 10b [154]. Yao et al. also developed FEC-based electrolyte LITFSI, which shows limited capacity loss of up to 5.2% over 500 cycles at 4C [159].

Nan et al. used low-polarity-solvent electrolytes (2.0 M LiFSI-EMC/TTE) to improve the Li^+ ion charge transfer kinetics between electrode–electrolyte interfaces at low temperatures. Their result showed that this electrolyte permits the NMC811||Gr cell to function in a broad temperature range from 25 °C to −20 °C with an 81% discharge capacity re-

tention [160–162]. A few works have been published on adding esters such as methyl acetate (MA) to the $LiPF_6$-based carbonate electrolyte and have demonstrated stabilized fast-charge cycling performance, increased overall conductivity, and reduced electrolyte viscosity [163,164].

5.2. SEI Layer Modification

SEI layer modification is another chemical-based approach to minimizing plating by introducing an engineered solid–electrolyte interface (SEI) layer at the anode surface. Extensive research has been conducted on developing a solid–electrolyte interface in lithium metal batteries [165]. Xinyang et al. showed that localized high-concentration electrolyte induces a LiF-rich SEI layer on the graphite anode. This inorganic SEI layer controls the lithium intercalating diffusion flux across the electrode, as shown in Figure 10a. The LiF-rich SEI also has an advantage due to its high Young's modulus, which also mechanically inhibits dendritic formation on the anode surface by restricting the volume expansion during plating. This lower change in anode surface area provides uniform Li^+ flux during fast charging, showcasing high reversibility (84.4% capacity retention) and nearly stable coulombic efficiency (Figure 10a) over 150 cycles [153].

Table 4. Different mitigation strategies for lithium plating.

Type of Factor	Mechanism	Effectivity and Limitation	Ref
Solvation Behavior Modification	Changing the chemical composition of the electrolyte by adding methyl acetate, fluorobenzene-based electrolyte, and acetonitrile solvents to form a stable SEI layer that can transport lithium quicker and enhance the desolvation process.	Ensured better-charged transfer at low temperatures and fast charging rates. The higher cost of production limits its application. It is also challenging to find strongly bound solvents for lithium ions.	[148,150,151]
Additive Addition to the Electrolyte	Additives (LIBFEP, LPSE) act as a deoxidizing agent in the electrolyte, and they (a) accelerate lithium-ion transport at the interface and (b) suppress its dendritic growth. In addition, additives also help (c) to reduce viscosity and (d) improve the transference number of the electrolyte.	It improves the coulombic efficiency and, eventually, higher capacity retention after fast cycling. It also (a) improves high charging rate performance, (b) increases ionic conductivity, and (c) enhances low-temperature performance. This eventually replicates into higher capacity retention, increased power densities, and reduced anodic interface resistance. However, this process is costly and not suitable for larger scales. Adulterated electrolytes sometimes react with the current collector and generate gases. It still needs to be commercially used and needs proper optimization.	[158–164,166–170]
SEI Layer Modification	Artificially formed LIF-rich, thin SEI layer controls the lithium flux and mechanically inhibits dendritic plating.	It improves cycling efficiency during fast charging. More literature is needed in this direction.	[153,165]
AC Pulse Charging	Application of the alternating pulse current relaxes charge polarization, which ultimately reduces plating. Pulse heating generates heat and provides an optimum temperature for charging.	Pulse charging has the potential for rapid adaptability. However, limitations included the unavailability of low-cost ICs for switching high currents. Pulse heating is still limited in lab-scale studies.	[43,155,171–174]
Adaptive Charging Strategy	Variable charging rates in real time using a feedback controller.	Adaptive charging has great potential, but the current application is limited due to the unavailability of a cheap, fast, and intelligent feedback controller.	[126,145,175]

Table 4. *Cont.*

Type of Factor	Mechanism	Effectivity and Limitation	Ref
Externally Applied Field	External magnetic field affected the movement of charged lithium ion due to Lorentz force and reduced the non-uniformity in lithium plating.	Research shows it can result in significant capacity gain. More literature is needed in this direction.	[135,176,177]
Surface Engineering	Engineered pore increases anode porosity. Sometimes, making a flexible ionic transport channel reduces the charge overpotential and limits the plating.	This method is still far from commercial use due to its customization.	[156,157,178–181]
Internal Heating Arrangement	Adding an external heating element into the battery enhances the electrolyte mobility and electrode kinetics.	It shows minimal degradation. The main drawback of this design is the addition of an extra heating element to the cell design, which increases the cost and weight. Cell fabrication also has a critical role to play.	[42,182]

5.3. Alternating Current Pulse Charging and Pulse Heating

During conventional CC-CV fast charging, lithium ions accumulated at the anode interface causing the anode potential to drop. Hence, to mitigate plating during fast charging, Jeong et al. used the idea of intermittent charging. They provided a specific rest period between each high C rate pulse, allowing some time to redistribute accumulated lithium ions at the anode–electrolyte interface, eventually reducing cell polarization. They compared the result of 6C pulse charging with 4C CC-CV charging measurement. Figure 10d shows higher coulombic efficiency and lesser plating loss in the case of pulse charging compared to conventional charging [43,155]. Qin et al. charged a battery quickly using pulse charging at lower temperatures till 3C at 0 °C and 1.5C at −10 °C without plating deposition [173]. Wu et al. also reported the linear capacity loss as an effect of high temperature on pulse charging applications [174]. This signifies the limitation of implementing a pulse charging strategy during mass application. Furthermore, integrating ICs with pulse charging capability needs a complex control algorithm to ensure the safe operation of the charger, which eventually requires a high cost for implementation.

On the other hand, lithium plating dominates as a nonlinear accelerated aging mechanism when the average charging temperature is below 30 °C [174]. Hence, the battery is heated via an electrochemical process by applying an external current that produces a steady temperature increase inside the battery [171,182]. The heating caused by high charging/discharging currents and AC (alternative current) pulses is considered as internal heating. Continuous current heating causes a significant SOC and SOH fall, even though it can swiftly raise the battery temperature. Conversely, AC pulse heating shows minimal SOH decrease. The power loss of AC pulse heating is also significantly lower than that of continuous current heating [172]. Li et al. developed a physics-based AC pulse heating protocol to estimate the potential of the negative electrode and battery internal temperature evolution. The result showed a significant reduction in lithium plating nucleation [140]. More research must be carried out to understand the interaction of the various physical parameters during pulse heating.

5.4. Adaptive Charging Strategy

Other charging strategies have been developed in the last few years. These are feedback loop-based dynamic charging methods. Katzer et al. proposed the idea of an adaptive fast-charging strategy using an impedance-based feedback loop. This method controls the charging rates with output from impedance results [66,126]. In this method, the cell is initially forced to be charged marginally above the kinetic limitation of anodic charge transfer. Then, it will move to the regulated charging current regime controlled by the prior

impedance-based result related to the onset of the lithium plating. Their result showcased the high efficacy of this method, with +46% faster charging and a mild degradation rate of 1.29% compared to standard CC-CV charging. This charging strategy can be a suitable, highly efficient, and reliable plating reduction method [175].

Zoerr. et al. used a similar polarization-based charging strategy to mitigate plating using a linear correlation with cell voltage and anode potential. The voltage threshold, plating SOC, and onset time were decided with an electrochemical model that kept the anodic potential above 10.0 mV. The model output was used in a feedback controller to control the charging rate so that the anode voltage could be maintained above the threshold limit [145]. However, it has inherent limitations when processing a large set of data in short time intervals.

5.5. External Magnetic Field

Some researchers have published work on the effect of a charged lithium-ion under a magnetic field. They reported that the movement of Li^+ is affected by the external magnetic field. Kang et al. introduced external magnetic fields to suppress the dendritic growth of plated lithium. The external field helps to create the Lorentz force, producing a magnetohydrodynamics effect inside the Li-ion cell [176]. The charged lithium ions traveling parallel to the applied field's direction experience no MHD forces ($v \times B = 0$). This spiral motion of transverse lithium ions due to the Lorentz force eliminates the chances of charge localization and reduces the chance of dendritic formation on the lithium metal anode. Sarkar et al. also demonstrated the magnetohydrodynamics effect in the case of LCO/C cells during fast charging, causing uniform lithium deposition. They also showcased a significant increase in capacity retention up to 20% with a 5C fast charging rate under a magnetic field, as shown in Figure 10d [135].

5.6. Surface Engineering

5.6.1. Surface Channeling

Researchers found that acceleration of solid-state diffusion, particularly in the anodes, can lower polarization by keeping the anode potential away from plating nucleation [178–183]. The previous literature suggests that lower particle size and thinner anode thickness decrease the plating tendency of the graphite electrode [69]. Researchers at Shandong University created a unique solution to increase the solid-state diffusion pathway in lithium-ion batteries. They utilized graphdiyne (GDY) as the anode material for fast charging with self-expanding lithium-ion transport channels. These channels lowered the energy barrier for Li^+ transport in the GDY electrode. The mechanism behind self-expansion is possibly due to the Li^+-π interaction, which induces reversible alkyne–alkene complex transition during the anode intercalation process. The out-of-plane Li^+-ion migration to stimulate solid-state lithium diffusion through the expanded channels is driven by the reciprocal repulsion of the adsorbed Li^+ at the conjugate sites of benzene rings and butadiyne triangular-like pores. Figure 10e schematically shows the ease of ion transport in the expanded channel and the corresponding 93% capacity retention at 3C over 500 cycles, as shown in Figure 10e [156].

Adapting the electrode architecture to control tortuosity is another way to boost active material use and increase high-rate capabilities. Goel et al. created highly ordered laser-patterned electrodes with vertical pores to facilitate quick lithium-ion transport through graphite electrodes. This pattern exposes the larger surface area for lithium intercalation, eventually reducing lithium flux and plating [184]. The size of an electrode increased for the same power density due to the presence of a hole acting as a limitation during application. Sander et al. proposed aligning the pore with external magnetic force inside the graphite particle. This formed directed pores, allowing quicker charge transport kinetics [179]. Parikh et al. created a low-tortuosity electrode with high structural stability, leading to shorter diffusion routes using a scalable frozen tape cast (FTC) technique. Compared to the conventionally coated electrode at 5C, the bilayer hybrid FTC electrode demonstrated a

20% increase in specific charge capacity, indicating exceptional rate performance in cases of extremely fast charging [180]. Toigo et al. demonstrated a 12% increase in capacity retention with 3C charging after 100 cycles using a galvanic 3D structured Cu collector attached to an LTO electrode [16].

5.6.2. Gradient Porosity Distribution

In addition to kinetics, mass transport to the anode also plays a critical role during fast charging [185]. Yang and his colleagues successfully integrated the porosity gradient (high porosity in the top layer and low porosity in the bottom layer) to increase the mass transport into a thick, three-layered graphite electrode [157,181]. This engineered porous structure facilitated Li-ion transportation and improved overall cell performance even at rates up to 4C. In addition, cells with a three-layered porous structure show a much longer cyclic life than single-layer anode (Figure 10f) [59,157]. There are some reports on surface improvement to eliminate mechanical surface defects, such as placing higher disorder graphite structure at the electrode–electrolyte interface to reduce the chances of dendritic formation [63]. Here, it is important to mention that a few research groups utilized irreversible plating deposition during fast charging due to mass transport limitation as a lithium concentration method for the lithium recycling of commercially used end-of-life batteries [185,186]. Hence, anode porosity enhancement and structural modification also could affect the efficacy of those methods.

5.7. Internal Heating Arrangement

Earlier discussion showed a reduced plating tendency of lithium-ion cells at high temperatures. Chao-Yang's group reported a solution for lithium plating using a customizable cell with a heating attachment, as shown in Figure 10g. They showcased that the plating phenomenon can easily be reduced if cells are heated above 50 °C before charging. They used an external circuit element to control the temperature before charging to achieve a plating-free operation for low-temperature charging or fast-charging applications. This group also designed a customized cell with a nickel heating element. Their invention offered a practical solution for the eradication of dead lithium plating through a regulated state of charge (SOC) and elevated cell operating temperatures, resulting in a significant enhancement of cyclic life up to 4500 cycles at a 3.5C rate (Figure 10g) [42,182]. The addition of extra heating elements and incomplete charging are some of the limitations of this method. On the other hand, Haijun et al. proposed the idea of an initial rapid heating of the cell for a small duration; then, they proceeded to charge it at a low-temperature. Their work showed a capacity retention of 98.6% for 500 cycles [182].

6. Conclusions

This paper summarized the reported studies on several aspects of plating. The rapid capacity drop of LiBs is the primary concern for the industry, which limits their use in fast and low-temperature charging applications. Various electrochemical side reactions further complicate the safe operation's criticality during rapid charging. Lithium plating is the main contributor to capacity loss during fast and low-temperature charging, and it also has other secondary effects, such as the reaction with electrolytes and the production of gas inside the battery. Hence, the challenges due to plating are a significant concern for the battery community.

In this review, we incorporated the investigations reported during this decade on different conditions for plating and their underlying mechanisms, electrochemical detection techniques, and mitigation strategies. We reviewed different conditions that impact lithium plating. We briefly described the plating mechanism using kinetics and thermodynamics behavior for various situations. This discussion is also concise with regard to how different variables accelerate or decelerate plating. This discussion also explains the internal dynamics of each variable and the mitigation techniques. In this review, our focus is mainly on the electrochemical in situ detection techniques because of their potential for

future utilization in a BMS system. There are different electrochemical strategies available to detect lithium plating. However, only some promising detection methods can work in real time and provide quantifiable outcomes on lithium plating. Although they have limitations, they have a bright future in terms of their potential utilization in mass applications. Further investigation is needed in this direction to improve the electrochemical base characterization methods.

In addition, we reviewed the different reported physics-based and data-driven modeling approaches and their efficacy. Models can be used as predictive tools for lithium plating under various conditions. The discussion also includes the limitations of both types of modeling approaches. Future research on creating quick and intelligent optimal charging methods based on physics-informed adaptive learning approaches looks promising. This review also incorporates different mitigation strategies that can be incorporated in batteries to mitigate lithium plating. This review includes the optimization of electrolyte composition, engineered electrode structure and interface, external application of a magnetic field, external heating, and improved charging protocol. Before introducing them in the mass applications, electrolytes or additives must be tested in all extreme cases. Currently, all the compounds are tested at a basic lab scale. The application of the external magnetic field also looks promising, but efficiency is relatively low, and more study is needed in this direction. The specialized anode also comes with the inherent limitations of the specialized material design during manufacturing. It also increased the production cost and led to manufacturing challenges because customized techniques, such as patterning, tape casting, and artificial priority distribution, require specialized tools to produce the final product. On the other hand, the structure's integrity is also a significant concern due to its highly porous nature. All development work should consider the fact that the battery must remain stable under different temperatures and extreme mechanical (external loading, vibrational) conditions. Customization of the manufacturing system for the electrode with 3D architecture is another big challenge. On the other side, adding a heating element is a commercially viable option, but extra weight, cost, and incomplete charging are some of its current limitations. Out of all the possible alternatives, this internal heating method has shown a promising future for mass applications. This method uses initial heating up to a specific temperature to ensure zero plating susceptibility during fast or low-temperature charging. This is an excellent advantage in terms of scaling and wide deployment for electric vehicle manufacturers, considering its high efficacy of 80% state of charge retention for more than 4000 cycles during fast C rate cycling.

These developed techniques to prevent lithium plating during charging require further advancement in different extreme situations. Developing cutting-edge detection techniques that are simpler to utilize in engineering applications but can provide an in-depth understanding of the lithium plating mechanism under various operational conditions can be very useful and will eventually help the scientific community to design a better system that significantly limits degradation during rapid charging and achieves long-term service life goals.

Author Contributions: Conceptualization, S.D. and P.S.; methodology, S.D.; software, S.D.; investigation, S.D.; resources, S.D. and P.S.; data curation, S.D.; writing—original draft preparation, S.D.; writing—review and editing, S.D. and P.S.; visualization, S.D.; supervision, P.S.; project administration, P.S.; funding acquisition, P.S. All authors have read and agreed to the published version of the manuscript.

Funding: This work was partially supported by the U. S. National Science Foundation through Grant Number: 2203990. Other support for the work was from Iowa Energy Center through Grant 22-IEC-002 and by the Manorama and Shyam Bahadur Professorship of Iowa State University.

Acknowledgments: The guidance and discussion with Anirudha Karati and Cajetan I Nlebedim from Ames National Lab are also gratefully acknowledged. William C Manor and Nicholas R Lueder, undergraduate students from Iowa State University, helped collect data for Tables 3 and 4.

Conflicts of Interest: The authors declare no competing financial interests.

Nomenclature

α, β = Constant
I = Current density
k = Kinetic constant
c = Lithium concentration
F = Faraday number
T = Temperature
$\mathcal{R}$ = **Universal gas constant**
η = **Overpotential**
U_{OCP} = Open circuit potential
$\mathbb{R}$ = **Resistance**
m = Mass of plated material
suffix
e = Electrolyte
s = Solid
n = Negative electrode
pl = Plating
st = Stripping
el = Intercalating
surf = Surface

References

1. Delmotte, V.M.; Zhai, P.; Pirani, A.; Connors, S.L.; Pean, C.; Chen, Y.; Goldfarb, L.; Gomis, M.I.; Mathews, J.B.R.; Berger, S.; et al. *Climate Change 2021: The Physical Science Basis*; Contribution of Working Group I to the IPCC Sixth Assessment Report; Cambridge University Press: Cambridge, UK, 2021.
2. UN Climate Press Release. COP28 Agreement Signals "Beginning of the End" of the Fossil Fuel Era. 2023. Available online: https://unfccc.int/news/cop28-agreement-signals-beginning-of-the-end-of-the-fossil-fuel-era (accessed on 8 April 2024).
3. Xiong, R.; Sun, F.; He, H.; Nguyen, T.D. A data-driven adaptive state of charge and power capability joint estimator of lithium-ion polymer battery used in electric vehicles. *Energy* **2013**, *63*, 295–308. [CrossRef]
4. Pathak, P.K.; Gupta, A.R. Battery Energy Storage System. In Proceedings of the 2018 4th International Conference on Computational Intelligence & Communication Technology (CICT), Ghaziabad, India, 9–10 February 2018.
5. Diouf, B.; Pode, R. Potential of lithium-ion batteries in renewable energy. *Renew. Energy* **2015**, *76*, 375–380. [CrossRef]
6. Das, S.; Banerjee, T.; Mondal, N. A Comparative CFD Study to Analyze the Performance of NACA 0018 and S1210 Darrieus Wind Turbine Blade. In *Fluid Mechanics and Fluid Power (Vol. 2)*; Springer Nature: Singapore, 2023; pp. 279–284.
7. Slinger, K. Electrical Batteries for Renewable Energy. 2015. Available online: https://sites.tufts.edu/eeseniordesignhandbook/2015/electrical-batteries-for-renewable-energy/ (accessed on 10 April 2024).
8. Nitta, N.; Wu, F.; Lee, J.T.; Yushin, G. Li-ion battery materials: Present and future. *Mater. Today* **2015**, *18*, 252–264. [CrossRef]
9. Abraham, K.M. How Comparable Are Sodium-Ion Batteries to Lithium-Ion Counterparts? *ACS Energy Lett.* **2020**, *5*, 3544–3547. [CrossRef]
10. Masias, A.; Marcicki, J.; Paxton, W.A. Opportunities and Challenges of Lithium Ion Batteries in Automotive Applications. *ACS Energy Lett.* **2021**, *6*, 621–630. [CrossRef]
11. Frith, J.T.; Lacey, M.J.; Ulissi, U. A non-academic perspective on the future of lithium-based batteries. *Nat. Commun.* **2023**, *14*, 420. [CrossRef]
12. Belgibayeva, A.; Rakhmetova, A.; Rakhatkyzy, M.; Kairova, M.; Mukushev, I.; Issatayev, N.; Kalimuldina, G.; Nurpeissova, A.; Sun, Y.-K.; Bakenov, Z. Lithium-ion batteries for low-temperature applications: Limiting factors and solutions. *J. Power Sources* **2023**, *557*, 232550.
13. El Haj Assad, M.; Khosravi, A.; Malekan, M.; Rosen, M.A.; Nazari, M.A. Chapter 14—Energy storage. In *Design and Performance Optimization of Renewable Energy Systems*; Assad, M.E.H., Rosen, M.A., Eds.; Academic Press: Cambridge, MA, USA, 2021; pp. 205–219.
14. Yin, Y.; Shen, C.; Yturriaga, S.; Zheng, J. The Power-Energy Coupling Effect of Mixed Hard-Carbon/Graphite Anode. *J. Mater. Sci. Chem. Eng.* **2021**, *9*, 16–31. [CrossRef]
15. Birrozzi, A.; Copley, M.; Zamory, J.V.; Pasqualini, M.; Calcaterra, S.; Nobili, F.; Cicco, A.D.; Rajantie, H.; Briceno, M.; Bilbe, E.; et al. Scaling up "Nano" $Li_4Ti_5O_{12}$ for High-Power Lithium-Ion Anodes Using Large Scale Flame Spray Pyrolysis. *J. Electrochem. Soc.* **2015**, *162*, A2331. [CrossRef]
16. Toigo, C.; Frankenberger, M.; Billot, N.; Pscherer, C.; Stumper, B.; Distelrath, F.; Schubert, J.; Pettinger, K.H.; Arbizzani, A. Improved $Li_4Ti_5O_{12}$ electrodes by modified current collector surface. *Electrochim. Acta* **2021**, *392*, 138978. [CrossRef]
17. Xiong, Z.; Yun, Y.S.; Jin, H.-J. Applications of Carbon Nanotubes for Lithium Ion Battery Anodes. *Materials* **2013**, *6*, 1138. [CrossRef]

18. Manthiram, A. An Outlook on Lithium Ion Battery Technology. *ACS Cent. Sci.* **2017**, *3*, 1063–1069. [CrossRef] [PubMed]
19. Klett, M.; Eriksson, R.; Groot, J.; Svens, C.; Högström, K.; Lindström, R.W.; Berg, H.; Gustafson, T.; Lindbergh, G.; Edström, K. Non-uniform aging of cycled commercial $LiFePO_4$//graphite cylindrical cells revealed by post-mortem analysis. *J. Power Sources* **2014**, *257*, 126–137. [CrossRef]
20. Janakiraman, U.; Garrick, T.R.; Fortier, M.E. Review—Lithium Plating Detection Methods in Li-Ion Batteries. *J. Electrochem. Soc.* **2020**, *167*, 160552. [CrossRef]
21. Qiu, Y.; Zhang, X.; Usubelli, C.; Mayer, D.; Linder, C.; Christensen, J. Understanding thermal and mechanical effects on lithium plating in lithium-ion batteries. *J. Power Sources* **2022**, *541*, 231632. [CrossRef]
22. Bach, T.C.; Schuster, S.F.; Fleder, E.; Müller, J.; Brand, M.J.; Lorrmann, H.; Jossen, A.; Sextl, G. Nonlinear aging of cylindrical lithium-ion cells linked to heterogeneous compression. *J. Energy Storage* **2016**, *5*, 212–223. [CrossRef]
23. Broussely, M.; Herreyre, S.; Biensan, P.; Kasztejna, P.; Nechev, K.; Staniewicz, R.J. Aging mechanism in Li ion cells and calendar life predictions. *J. Power Sources* **2001**, *97*, 13–21. [CrossRef]
24. Zhou, J.; Notten, P.H.L. Studies on the degradation of Li-ion batteries by the use of microreference electrodes. *J. Power Sources* **2008**, *177*, 553–560. [CrossRef]
25. Grolleau, S.; Delaille, A.; Gualous, H.; Gyan, P.; Revel, R.; Bernard, J.; Redondo-Iglesias, E.; Peter, J. Calendar aging of commercial graphite/$LiFePO_4$ cell—Predicting capacity fade under time dependent storage conditions. *J. Power Sources* **2014**, *255*, 450–458. [CrossRef]
26. Liu, J.; Zhang, Y.; Bai, J.; Zhou, L.; Wang, Z. Influence of lithium plating on lithium-ion battery aging at high temperature. *Electrochim. Acta* **2023**, *454*, 142362. [CrossRef]
27. Wang, Y.; Chang, X.; Li, Z.; Mei, Y.; Zhang, Y.; Liu, L.; Wang, K.; Gu, H.; Li, L. Preventing Sudden Death of High-Energy Lithium-Ion Batteries at Elevated Temperature Through Interfacial Ion-Flux Rectification. *Adv. Funct. Mater.* **2023**, *33*, 2208329. [CrossRef]
28. Choi, J.; Manthiram, A. Role of Chemical and Structural Stabilities on the Electrochemical Properties of Layered $LiNi_{1/3}Mn_{1/3}Co_{1/3}O_2$ Cathodes. *J. Electrochem. Soc.* **2005**, *152*, A1714. [CrossRef]
29. Choi, N.-S.; Yeon, J.-T.; Lee, Y.-W.; Han, J.-G.; Lee, K.T.; Kim, S.-S. Degradation of spinel lithium manganese oxides by low oxidation durability of LiPF6-based electrolyte at 60 °C. *Solid State Ion.* **2012**, *219*, 41–48. [CrossRef]
30. Downie, L.E.; Krause, L.J.; Burns, J.C.; Jensen, L.D.; Chevrier, V.L.; Dahn, J.R. In Situ Detection of Lithium Plating on Graphite Electrodes by Electrochemical Calorimetry. *J. Electrochem. Soc.* **2013**, *160*, A588–A594. [CrossRef]
31. Petzl, M.; Kasper, M.; Danzer, M.A. Lithium plating in a commercial lithium-ion battery A low-temperature aging study. *J. Power Sources* **2015**, *275*, 799–807. [CrossRef]
32. Cannarella, J.; Arnold, C.B. Stress evolution and capacity fade in constrained lithium-ion pouch cells. *J. Power Sources* **2014**, *245*, 745–751. [CrossRef]
33. Sarkar, A.; Shrotriya, P.; Nlebedim, I.C. Anodic interfacial evolution in extremely fast charged lithium-ion batteries. *ACS Appl. Energy Mater.* **2022**, *5*, 3179–3188. [CrossRef]
34. Ruess, R.; Schweidler, S.; Hemmelmann, H.; Conforto, G.; Bielefeld, A.; Weber, D.A.; Sann, J.; Elm, M.T.; Janek, J. Influence of NCM Particle Cracking on Kinetics of Lithium-Ion Batteries with Liquid or Solid Electrolyte. *J. Electrochem. Soc.* **2020**, *167*, 100532. [CrossRef]
35. Aurbach, D.; Markovsky, B.; Rodkin, A.; Cojocaru, M.; Levi, E.; Kim, H.-J. An analysis of rechargeable lithium-ion batteries after prolonged cycling. *Electrochim. Acta* **2002**, *47*, 1899–1911. [CrossRef]
36. Amatucci, G.G.; Tarascon, J.M.; Klein, L.C. Cobalt dissolution in LiCoO2-based non-aqueous rechargeable batteries. *Solid State Ion.* **1996**, *83*, 167–173. [CrossRef]
37. Arora, P.; White, R.E.; Doyle, M. Capacity Fade Mechanisms and Side Reactions in Lithium-Ion Batteries. *J. Electrochem. Soc.* **1998**, *145*, 3647. [CrossRef]
38. Guo, L.; Thornton, D.B.; Koronfel, M.A.; Stephens, I.E.L.; Ryan, M.P. Degradation in lithium ion battery current collectors. *J. Phys. Energy* **2021**, *3*, 032015.
39. Vetter, J.; Novak, P.; Wagner, M.R.; Veit, C.; Moller, K.C.; Besenhard, J.O.; Winter, M.; Wohlfahrt-Mehrens, M.; Vogler, C.; Hammouche, A. Ageing mechanisms in lithium-ion batteries. *J. Power Sources* **2005**, *147*, 269–281. [CrossRef]
40. Lin, X.K.; Khosravinia, K.; Hu, X.S.; Li, J.; Lu, W. Lithium Plating Mechanism, Detection, and Mitigation in Lithium-Ion Batteries. *Prog. Energy Combust. Sci.* **2021**, *87*, 100953. [CrossRef]
41. Burns, J.C.; Stevens, D.A.; Dahn, J.R. In-situ detection of lithium plating using high precision coulometry. *J. Electrochem. Soc.* **2015**, *162*, A959–A964. [CrossRef]
42. Yang, X.-G.; Zhang, G.; Ge, S.; Wang, C.-Y. Fast charging of lithium-ion batteries at all temperatures. *Proc. Natl. Acad. Sci. USA.* **2018**, *115*, 7266–7271. [CrossRef]
43. Purushothaman, B.K.; Landau, U. Rapid Charging of Lithium-Ion Batteries Using Pulsed Currents: A Theoretical Analysis. *J. Electrochem. Soc.* **2006**, *153*, A533. [CrossRef]
44. Chen, Y.; Chen, K.-H.; Sanchez, A.J.; Kazyak, E.; Goel, V.; Gorlin, Y.; Christensen, J.; Thornton, K.; Dasgupta, N.P. Operando video microscopy of Li plating and re-intercalation on graphite anodes during fast charging. *J. Mater. Chem. A* **2021**, *9*, 23522–23536. [CrossRef]

45. Gao, T.; Han, Y.; Fraggedakis, D.; Das, S.; Zhou, T.; Yeh, C.-N.; Xu, S.; Chueh, W.C.; Li, J.; Bazant, M.Z. Interplay of Lithium Intercalation and Plating on a Single Graphite Particle. *Joule* **2021**, *5*, 393–414. [CrossRef]
46. Sarkar, A.; Nlebedim, I.C.; Shrotriya, P. Performance degradation due to anodic failure mechanisms in lithium-ion batteries. *J. Power Sources* **2021**, *502*, 229145. [CrossRef]
47. Xie, Y.; Wang, S.; Li, R.; Ren, D.; Yi, M.; Xu, C.; Han, X.; Lu, L.; Friess, B.; Offer, G.; et al. Inhomogeneous degradation induced by lithium plating in a large-format lithium-ion battery. *J. Power Sources* **2022**, *542*, 231753. [CrossRef]
48. Liu, J.; Wang, Z.; Bai, J. Influences of multi factors on thermal runaway induced by overcharging of lithium-ion battery. *J. Energy Chem.* **2022**, *70*, 531–541. [CrossRef]
49. Lyu, P.; Liu, X.; Qu, J.; Zhao, J.; Huo, Y.; Qu, Z.; Rao, Z. Recent advances of thermal safety of lithium ion battery for energy storage. *Energy Storage Mater.* **2020**, *31*, 195–220. [CrossRef]
50. Wang, B.; Le Fevre, L.W.; Brookfield, A.; McInnes, E.J.L.; Dryfe, R.A.W. Resolution of Lithium Deposition versus Intercalation of Graphite Anodes in Lithium Ion Batteries: An In Situ Electron Paramagnetic Resonance Study. *Angew. Chem. Int. Ed.* **2021**, *60*, 21860–21867. [CrossRef]
51. Wang, C.; Yang, C.; Zheng, Z. Toward Practical High-Energy and High-Power Lithium Battery Anodes: Present and Future. *Adv. Sci.* **2022**, *9*, 2105213. [CrossRef]
52. Rangarajan, S.P.; Fear, C.; Adhikary, T.; Barsukov, Y.; Dadheech, G.; Mukherjee, P.P. Dynamics of lithium stripping on graphite electrodes after fast charging. *Cell Rep. Phys. Sci.* **2023**, *4*, 101740. [CrossRef]
53. Keyser, M.; Pesaran, A.; Li, Q.; Santhanagopalan, S.; Smith, K.; Wood, E.; Ahmed, S.; Bloom, I.; Dufek, E.; Shirk, M.; et al. Enabling fast charging—Battery thermal considerations. *J. Power Sources* **2017**, *367*, 228–236. [CrossRef]
54. Gargh, P.P.; Sarkar, A.; Nlebedim, I.C.; Shrotriya, P. Lithium plating induced degradation during fast charging of batteries subjected to compressive loading. *J. Energy Storage* **2024**, *84*, 110701. [CrossRef]
55. Kurzweil, P.; Scheuerpflug, W.; Frenzel, B.; Schell, C.; Schottenbauer, J. Differential Capacity as a Tool for SOC and SOH Estimation of Lithium Ion Batteries Using Charge/Discharge Curves, Cyclic Voltammetry, Impedance Spectroscopy, and Heat Events: A Tutorial. *Energies* **2022**, *15*, 4520. [CrossRef]
56. Xiong, Y.; Liu, Y.; Chen, L.; Zhang, S.; Zhu, X.; Shen, T.; Ren, D.; He, X.; Qiu, J.; Wang, L.; et al. New Insight on Graphite Anode Degradation Induced by Li-Plating. *Energy Environ. Mater.* **2022**, *5*, 872–876. [CrossRef]
57. Li, Y.; Feng, X.; Ren, D.; Ouyang, M.; Lu, L.; Han, Z. Thermal Runaway Triggered by Plated Lithium on the Anode after Fast Charging. *ACS Appl. Mater. Interfaces* **2019**, *11*, 46839–46850. [CrossRef]
58. Gargh, P.; Sarkar, A.; Lui, Y.H.; Shen, S.; Hu, C.; Hu, S.; Nlebedim, I.C.; Shrotriya, P. Correlating capacity fade with film resistance loss in fast charging of lithium-ion battery. *J. Power Sources* **2021**, *485*, 229360. [CrossRef]
59. Birkenmaier, C.; Bitzer, B.; Harzheim, M.; Hintennach, A.; Schleid, T. Lithium Plating on Graphite Negative Electrodes: Innovative Qualitative and Quantitative Investigation Methods. *J. Electrochem. Soc.* **2015**, *162*, A2646. [CrossRef]
60. Fonseca Rodrigues, M.-T.; Maroni, V.A.; Gosztola, D.J.; Yao, K.P.C.; Kalaga, K.; Shkrob, I.A.; Abraham, D.P. Lithium Acetylide: A Spectroscopic Marker for Lithium Deposition During Fast Charging of Li-Ion Cells. *ACS Appl. Energy Mater.* **2019**, *2*, 873–881. [CrossRef]
61. Tang, Y.; Shen, K.; Lv, Z.; Xu, X.; Hou, G.; Cao, H.; Wu, L.; Zheng, G.; Deng, Y. Three-dimensional ordered macroporous Cu current collector for lithium metal anode: Uniform nucleation by seed crystal. *J. Power Sources* **2018**, *403*, 82–89. [CrossRef]
62. Xie, W.; Liu, X.; He, R.; Li, Y.; Gao, X.; Li, X.; Peng, Z.; Feng, S.; Feng, X.; Yang, S. Challenges and opportunities toward fast-charging of lithium-ion batteries. *J. Energy Storage* **2020**, *32*, 101837. [CrossRef]
63. Honbo, H.; Takei, K.; Ishii, Y.; Nishida, T. Electrochemical properties and Li deposition morphologies of surface modified graphite after grinding. *J. Power Sources* **2009**, *189*, 337–343. [CrossRef]
64. Lin, H.P.; Chua, D.; Salomon, M.; Shiao, H.C.; Hendrickson, M.; Plichta, E.; Slane, S. Low-Temperature Behavior of Li-Ion Cells. *Electrochem. Solid-State Lett.* **2001**, *4*, A71. [CrossRef]
65. Sheng, L.; Wang, Q.; Liu, X.; Cui, H.; Wang, X.; Xu, Y.; Li, Z.; Wang, L.; Chen, Z.; Xu, G.-L.; et al. Suppressing electrolyte-lithium metal reactivity via Li+-desolvation in uniform nano-porous separator. *Nat. Commun.* **2022**, *13*, 172. [CrossRef]
66. Hogrefe, C.; Waldmann, T.; Hölzle, M.; Wohlfahrt-Mehrens, M. Direct observation of internal short circuits by lithium dendrites in cross-sectional lithium-ion in situ full cells. *J. Power Sources* **2023**, *556*, 232391. [CrossRef]
67. Schuster, S.F.; Bach, T.; Fleder, E.; Müller, J.; Brand, M.; Sextl, G.; Jossen, A. Nonlinear aging characteristics of lithium-ion cells under different operational conditions. *J. Energy Storage* **2015**, *1*, 44–53. [CrossRef]
68. Meyer, J.M.; Harrison, K.L.; Mukherjee, P.P.; Roberts, S.A. Developing a model for the impact of non-conformal lithium contact on electro-chemo-mechanics and dendrite growth. *Cell Rep. Phys. Sci.* **2023**, *4*, 101364. [CrossRef]
69. Sarkar, A.; Shrotriya, P.; Nlebedim, I.C. Parametric analysis of anodic degradation mechanisms for fast charging lithium batteries with graphite anode. *Comput. Mater. Sci.* **2022**, *202*, 110979. [CrossRef]
70. Wang, H.; Zhu, Y.; Kim, S.C.; Pei, A.; Li, Y.; Boyle, D.T.; Wang, H.; Zhang, Z.; Ye, Y.; Huang, W.; et al. Underpotential lithium plating on graphite anodes caused by temperature heterogeneity. *Proc. Natl. Acad. Sci. USA* **2020**, *117*, 29453–29461. [CrossRef] [PubMed]
71. Ahmed, S.; Bloom, I.; Jansen, A.N.; Tanim, T.; Dufek, E.J.; Pesaran, A.; Burnham, A.; Carlson, R.B.; Dias, F.; Hardy, K.; et al. Enabling fast charging—A battery technology gap assessment. *J. Power Sources* **2017**, *367*, 250–262. [CrossRef]

72. Hein, S.; Latz, A. Influence of local lithium metal deposition in 3D microstructures on local and global behavior of Lithium-ion batteries. *Electrochim. Acta* **2016**, *201*, 354–365. [CrossRef]
73. Swiderska-Mocek, A.; Rudnicka, E.; Lewandowski, A. Temperature coefficients of Li-ion battery single electrode potentials and related entropy changes—Revisited. *Phys. Chem. Chem. Phys.* **2019**, *21*, 2115–2120. [CrossRef]
74. Bazinski, S.J.; Wang, X. The Influence of Cell Temperature on the Entropic Coefficient of a Lithium Iron Phosphate (LFP) Pouch Cell. *J. Electrochem. Soc.* **2014**, *161*, A168. [CrossRef]
75. Takano, K.; Saito, Y.; Kanari, K.; Nozaki, K.; Kato, K.; Negishi, A.; Kato, T. Entropy change in lithium-ion cells on charge and discharge. *J. Appl. Electrochem.* **2002**, *32*, 251–258. [CrossRef]
76. Bai, P.; Li, J.; Brushett, F.R.; Bazant, M.Z. Transition of lithium growth mechanisms in liquid electrolytes. *Energy Environ. Sci.* **2016**, *9*, 3221–3229. [CrossRef]
77. Legrand, N.; Knosp, B.; Desprez, P.; Lapicque, F.; Rael, S. Physical characterization of the charging process of a Li-ion battery and prediction of Li plating by electrochemical modelling. *J. Power Sources* **2014**, *245*, 208–216. [CrossRef]
78. Bazant, M.Z. Thermodynamic stability of driven open systems and control of phase separation by electro-autocatalysis. *Faraday Discus.* **2017**, *199*, 423–463. [CrossRef] [PubMed]
79. Bazant, M.Z. Theory of Chemical Kinetics and Charge Transfer based on Nonequilibrium Thermodynamics. *Acc. Chem. Res.* **2013**, *46*, 1144–1160. [CrossRef] [PubMed]
80. Jiang, F.-N.; Yang, S.-J.; Liu, H.; Cheng, X.-B.; Liu, L.; Xiang, R.; Zhang, Q.; Kaskel, S.; Huang, J.-Q. Mechanism understanding for stripping electrochemistry of Li metal anode. *SusMat* **2021**, *1*, 506–536. [CrossRef]
81. Park, G.; Gunawardhana, N.; Nakamura, H.; Lee, Y.S.; Yoshio, M. The study of electrochemical properties and lithium deposition of graphite at low temperature. *J. Power Sources* **2012**, *199*, 293–299. [CrossRef]
82. Gao, X.; Li, S.; Xue, J.; Hu, D.; Xu, J. A Mechanistic and Quantitative Understanding of the Interactions between SiO and Graphite Particles. *Adv. Energy Mater.* **2023**, *13*, 2202584. [CrossRef]
83. Son, Y.; Cha, H.; Lee, T.; Kim, Y.; Boies, A.; Cho, J.; De Volder, M. Analysis of Differences in Electrochemical Performance Between Coin and Pouch Cells for Lithium-Ion Battery Applications. *Energy Environ. Mater.* **2023**, *7*, e12615. [CrossRef]
84. Spingler, F.B.; Friedrich, S.; Kücher, S.; Schmid, S.; López-Cruz, D.; Jossen, A. The Effects of Non-Uniform Mechanical Compression of Lithium-Ion Cells on Local Current Densities and Lithium Plating. *J. Electrochem. Soc.* **2021**, *168*, 110515. [CrossRef]
85. Wang, Y.; Zhang, C.; Hu, J.; Zhang, P.; Zhang, L.; Lao, L. Investigation on calendar experiment and failure mechanism of lithium-ion battery electrolyte leakage. *J. Energy Storage* **2022**, *54*, 105286. [CrossRef]
86. Deichmann, E.; Torres-Castro, L.; Lamb, J.; Karulkar, M.; Ivanov, S.; Grosso, C.; Gray, L.; Langendorf, J.; Garzon, F. Investigating the Effects of Lithium Deposition on the Abuse Response of Lithium-Ion Batteries. *J. Electrochem. Soc.* **2020**, *167*, 090552. [CrossRef]
87. Smith, A.J.; Fang, Y.; Mikheenkova, A.; Ekström, H.; Svens, P.; Ahmed, I.; Lacey, M.J.; Lindbergh, G.; Furó, I.; Lindström, R.W. Localized lithium plating under mild cycling conditions in high-energy lithium-ion batteries. *J. Power Sources* **2023**, *573*, 233118. [CrossRef]
88. Attia, P.M.; Bills, A.; Planella, F.B.; Dechent, P.; dos Reis, G.; Dubarry, M.; Gasper, P.; Gilchrist, R.; Greenbank, S.; Howey, D.; et al. Review—"Knees" in Lithium-Ion Battery Aging Trajectories. *J. Electrochem. Soc.* **2022**, *169*, 060517. [CrossRef]
89. Ecker, M.; Sabet, P.S.; Sauer, D.U. Influence of operational condition on lithium plating for commercial lithium-ion batteries—Electrochemical experiments and post-mortem-analysis. *Appl. Energy* **2017**, *206*, 934–946. [CrossRef]
90. Cannarella, J.; Arnold, C.B. The Effects of Defects on Localized Plating in Lithium-Ion Batteries. *J. Electrochem. Soc.* **2015**, *162*, A1365–A1373. [CrossRef]
91. Peabody, C.; Arnold, C.B. The role of mechanically induced separator creep in lithium-ion battery capacity fade. *J. Power Sources* **2011**, *196*, 8147–8153. [CrossRef]
92. Matasso, A.; Wetz, D.; Liu, F. The Effects of Internal Pressure Evolution on the Aging of Commercial Li-Ion Cells. *ECS Trans.* **2014**, *58*, 37. [CrossRef]
93. Pan, Y.; Zhong, Z. Modeling the Ion Transport Restriction in Mechanically Strained Separator Membranes. *J. Electrochem. Soc.* **2014**, *161*, A583. [CrossRef]
94. Antartis, D.; Dillon, S.; Chasiotis, I. Effect of porosity on electrochemical and mechanical properties of composite Li-ion anodes. *J. Compos. Mater.* **2015**, *49*, 1849–1862. [CrossRef]
95. Yao, F.; Güneş, F.; Ta, H.Q.; Lee, S.M.; Chae, S.J.; Sheem, K.Y.; Cojocaru, C.S.; Xie, S.S.; Lee, Y.H. Diffusion Mechanism of Lithium Ion through Basal Plane of Layered Graphene. *J. Am. Chem. Soc.* **2012**, *134*, 8646–8654. [CrossRef]
96. McShane, E.J.; Colclasure, A.M.; Brown, D.E.; Konz, Z.M.; Smith, K.; McCloskey, B.D. Quantification of Inactive Lithium and Solid–Electrolyte Interphase Species on Graphite Electrodes after Fast Charging. *ACS Energy Lett.* **2020**, *5*, 2045–2051. [CrossRef]
97. Tang, M.; Albertus, P.; Newman, J. Two-Dimensional Modeling of Lithium Deposition during Cell Charging. *J. Electrochem. Soc.* **2009**, *156*, A390. [CrossRef]
98. Yang, Y.; Xu, L.; Yang, S.-J.; Yan, C.; Huang, J.-Q. Electrolyte inhomogeneity induced lithium plating in fast charging lithium-ion batteries. *J. Energy Chem.* **2022**, *73*, 394–399. [CrossRef]
99. Dubarry, M.; Truchot, C.; Liaw, B.Y. Synthesize battery degradation modes via a diagnostic and prognostic model. *J. Power Sources* **2012**, *219*, 204–216. [CrossRef]
100. Zhou, H.; Fear, C.; Jeevarajan, J.A.; Mukherjee, P.P. State-of-electrode (SOE) analytics of lithium-ion cells under overdischarge extremes. *Energy Storage Mater.* **2023**, *54*, 60–74. [CrossRef]

101. Yin, T.; Jia, L.; Li, X.; Zheng, L.; Dai, Z. Effect of High-Rate Cycle Aging and Over-Discharge on NCM811 ($LiNi_{0.8}Co_{0.1}Mn_{0.1}O_2$) Batteries. *Energies* **2022**, *15*, 2862. [CrossRef]
102. Wang, L.; Xie, L.; Song, Y.; Liu, X.; Zhang, H.; He, X. Identifying cathode and anode polarizations during practical high-rate charging/discharging in different Li-ion pouch batteries. *Battery Energy* **2023**, *2*, 20220025. [CrossRef]
103. Mei, W.; Zhang, L.; Sun, J.; Wang, Q. Experimental and numerical methods to investigate the overcharge caused lithium plating for lithium ion battery. *Energy Storage Mater.* **2020**, *32*, 91–104. [CrossRef]
104. Louli, A.J.; Genovese, M.; Weber, R.; Hames, S.G.; Logan, E.R.; Dahn, J.R. Exploring the Impact of Mechanical Pressure on the Performance of Anode-Free Lithium Metal Cells. *J. Electrochem. Soc.* **2019**, *166*, A1291–A1299. [CrossRef]
105. Jaguemont, J.; Boulon, L.; Dube, Y.; Poudrier, D. Low Temperature Discharge Cycle Tests for a Lithium Ion Cell. In Proceedings of the 2014 IEEE Vehicle Power and Propulsion Conference (VPPC), Coimbra, Portugal, 27–30 October 2014.
106. Cho, H.-M.; Choi, W.-S.; Go, J.-Y.; Bae, S.-E.; Shin, H.-C. A study on time-dependent low temperature power performance of a lithium-ion battery. *J. Power Sources* **2012**, *198*, 273–280. [CrossRef]
107. Carter, R.; Kingston, T.A.; Atkinson, R.W.; Parmananda, M.; Dubarry, M.; Fear, C.; Mukherjee, P.P.; Love, C.T. Directionality of thermal gradients in lithium-ion batteries dictates diverging degradation modes. *Cell Rep. Phys. Sci.* **2021**, *2*, 100351. [CrossRef]
108. Zhang, G.; Shen, W.; Wei, X. Lithium-ion battery thermal safety evolution during high-temperature nonlinear aging. *Fuel* **2024**, *362*, 130845. [CrossRef]
109. Yuan, W.; Liang, D.; Chu, Y.; Wang, Q. Aging effect delays overcharge-induced thermal runaway of lithium-ion batteries. *J. Loss Prev. Process Ind.* **2022**, *79*, 104830. [CrossRef]
110. Zhao, L.; Zheng, M.; Zhang, J.; Liu, H.; Li, W.; Chen, M. Numerical modeling of thermal runaway for low temperature cycling lithium-ion batteries. *J. Energy Storage* **2023**, *63*, 107053. [CrossRef]
111. Aufschläger, A.; Durdel, A.; Kraft, L.; Jossen, A. Optimizing mechanical compression for cycle life and irreversible swelling of high energy and high power lithium-ion pouch cells. *J. Energy Storage* **2024**, *76*, 109883. [CrossRef]
112. Fang, C.; Lu, B.; Pawar, G.; Zhang, M.; Cheng, D.; Chen, S.; Ceja, M.; Doux, J.-M.; Musrock, H.; Cai, M.; et al. Pressure-tailored lithium deposition and dissolution in lithium metal batteries. *Nat. Energy* **2021**, *6*, 987–994. [CrossRef]
113. Lee, Y.K.; Shin, H. Modeling and simulation of a composite solid-state battery: The effects of stack pressure on electrochemical and mechanical behavior. *J. Energy Storage* **2024**, *78*, 110051. [CrossRef]
114. Cao, C.; Steinrück, H.-G.; Paul, P.P.; Dunlop, A.R.; Trask, S.E.; Jansen, A.N.; Kasse, R.M.; Thampy, V.; Yusuf, M.; Weker, J.N.; et al. Conformal Pressure and Fast-Charging Li-Ion Batteries. *J. Electrochem. Soc.* **2022**, *169*, 040540. [CrossRef]
115. Petzl, M.; Danzer, M.A. Nondestructive detection, characterization, and quantification of lithium plating in commercial lithium-ion batteries. *J. Power Sources* **2014**, *254*, 80–87. [CrossRef]
116. Waldmann, T.; Iturrondobeitia, A.; Kasper, M.; Ghanbari, N.; Aguesse, F.; Bekaert, E.; Daniel, L.; Genies, S.; Gordon, I.J.; Löble, M.W.; et al. Review—Post-Mortem Analysis of Aged Lithium-Ion Batteries: Disassembly Methodology and Physico-Chemical Analysis Techniques. *J. Electrochem. Soc.* **2016**, *163*, A2149. [CrossRef]
117. Harris, S.J.; Timmons, A.; Baker, D.R.; Monroe, C. Direct in situ measurements of Li transport in Li-ion battery negative electrodes. *Chem. Phys. Lett.* **2010**, *485*, 265–274. [CrossRef]
118. Zinth, V.; Von Lüders, C.; Hofmann, M.; Hattendorff, J.; Buchberger, I.; Erhard, S.; Rebelo-Kornmeier, J.; Jossen, A.; Gilles, R. Lithium plating in lithium-ion batteries at sub-ambient temperatures investigated by in situ neutron diffraction. *J. Power Sources* **2014**, *271*, 152–159. [CrossRef]
119. Niemoller, A.; Jakes, P.; Eichel, R.A.; Granwehr, J. EPR Imaging of Metallic Lithium and its Application to Dendrite Localisation in Battery Separators. *Sci. Rep.* **2018**, *8*, 14331. [CrossRef] [PubMed]
120. Ghassemi, H.; Au, M.; Chen, N.; Heiden, P.A.; Yassar, R.S. Real-time observation of lithium fibers growth inside a nanoscale lithium-ion battery. *Appl. Phys. Lett.* **2011**, *99*, 123113. [CrossRef]
121. Chen, G.; Zhuang, G.V.; Richardson, T.J.; Liu, G.; Ross, P.N. Anodic Polymerization of Vinyl Ethylene Carbonate in Li-Ion Battery Electrolyte. *Electrochem. Solid-State Lett.* **2005**, *8*, A344. [CrossRef]
122. Waldmann, T.; Ghanbari, N.; Kasper, M.; Wohlfahrt-Mehrens, M. Correlations between Electrochemical Data and Results from Post-Mortem Analysis of Aged Lithium-Ion Batteries. *J. Electrochem. Soc.* **2015**, *162*, A1500. [CrossRef]
123. Andre, D.; Meiler, M.; Steiner, K.; Walz, H.; Soczka-Guth, T.; Sauer, D.U. Characterization of high-power lithium-ion batteries by electrochemical impedance spectroscopy. II: Modelling. *J. Power Sources* **2011**, *196*, 5349–5356. [CrossRef]
124. Pastor-Fernández, C.; Widanage, W.D.; Marco, J.; Gama-Valdez, M.Á.; Chouchelamane, G.H. Identification and quantification of ageing mechanisms in Lithium-ion batteries using the EIS technique. In Proceedings of the 2016 IEEE Transportation Electrification Conference and Expo (ITEC), Dearborn, MI, USA, 27–29 June 2016.
125. Pastor-Fernandez, C.; Uddin, K.; Chouchelamane, G.H.; Widanage, W.D.; Marco, J. A Comparison between Electrochemical Impedance Spectroscopy and Incremental Capacity-Differential Voltage as Li-ion Diagnostic Techniques to Identify and Quantify the Effects of Degradation Modes within Battery Management Systems. *J. Power Sources* **2017**, *360*, 301–318. [CrossRef]
126. Koseoglou, M.; Tsioumas, E.; Ferentinou, D.; Jabbour, N.; Papagiannis, D.; Mademlis, C. Lithium plating detection using dynamic electrochemical impedance spectroscopy in lithium-ion batteries. *J. Power Sources* **2021**, *512*, 230508. [CrossRef]
127. Chen, X.; Li, L.Y.; Liu, M.M.; Huang, T.; Yu, A.S. Detection of lithium plating in lithium-ion batteries by distribution of relaxation times. *J. Power Sources* **2021**, *496*, 229867. [CrossRef]

128. Koleti, U.R.; Zhang, C.; Malik, R.; Dinh, T.Q.; Marco, J. The development of optimal charging strategies for lithium-ion batteries to prevent the onset of lithium plating at low ambient temperatures. *J. Energy Storage* **2019**, *24*, 100798. [CrossRef]
129. Yang, X.G.; Ge, S.; Liu, T.; Leng, Y.; Wang, C.Y. A look into the voltage plateau signal for detection and quantification of lithium plating in lithium-ion cells. *J. Power Sources* **2018**, *395*, 251–261. [CrossRef]
130. Tian, Y.; Lin, C.; Li, H.L.; Du, J.Y.; Xiong, R. Detecting undesired lithium plating on anodes for lithium-ion batteries-A review on the in-situ methods. *Appl. Energy* **2021**, *300*, 117386. [CrossRef]
131. Xu, L.; Xiao, Y.; Yang, Y.; Yang, S.-J.; Chen, X.-R.; Xu, R.; Yao, Y.-X.; Cai, W.-L.; Yan, C.; Huang, J.-Q.; et al. Operando Quantified Lithium Plating Determination Enabled by Dynamic Capacitance Measurement in Working Li-Ion Batteries. *Angew. Chem. Int. Ed.* **2022**, *61*, e202210365. [CrossRef] [PubMed]
132. Koseoglou, M.; Tsioumas, E.; Ferentinou, D.; Panagiotidis, I.; Jabbour, N.; Papagiannis, D.; Mademlis, C. Lithium plating detection using differential charging current analysis in lithium-ion batteries. *J. Energy Storage* **2022**, *54*, 105345. [CrossRef]
133. Safari, M.; Delacourt, C. Aging of a Commercial Graphite/$LiFePO_4$ Cell. *J. Electrochem. Soc.* **2011**, *158*, A1123. [CrossRef]
134. Fan, J.; Tan, S. Studies on charging lithium-ion cells at low temperatures. *J. Electrochem. Soc.* **2006**, *153*, A1081–A1092. [CrossRef]
135. Sarkar, A.; Shrotriya, P.; Nlebedim, I.C. Magnetohydrodynamic Control of Interfacial Degradation in Lithium-Ion Batteries for Fast Charging Applications. *ACS Appl. Mater. Interfaces* **2021**, *13*, 43606–43614. [CrossRef]
136. Doyle, M.; Fuller, T.F.; Newman, J. Modeling of Galvanostatic Charge and Discharge of the Lithium/Polymer/Insertion Cell. *J. Electrochem. Soc.* **1993**, *140*, 1526. [CrossRef]
137. Yang, K.; Zhang, L.; Zhang, Z.; Yu, H.; Wang, W.; Ouyang, M.; Zhang, C.; Sun, Q.; Yan, X.; Yang, S.; et al. Battery State of Health Estimate Strategies: From Data Analysis to End-Cloud Collaborative Framework. *Batteries* **2023**, *9*, 351. [CrossRef]
138. Arora, P.; Doyle, M.; White, R.E. Mathematical Modeling of the Lithium Deposition Overcharge Reaction in Lithium-Ion Batteries Using Carbon-Based Negative Electrodes. *J. Electrochem. Soc.* **1999**, *146*, 3543. [CrossRef]
139. Gao, Z.H.; Xie, H.C.; Yang, X.B.; Niu, W.F.; Li, S.; Chen, S.Y. The Dilemma of C-Rate and Cycle Life for Lithium-Ion Batteries under Low Temperature Fast Charging. *Batteries* **2022**, *8*, 234. [CrossRef]
140. Li, W.; Xie, Y.; Hu, X.; Tran, M.K.; Fowler, M.; Panchal, S.; Zheng, J.; Liu, K. An Internal Heating Strategy for Lithium-Ion Batteries Without Lithium Plating Based on Self-Adaptive Alternating Current Pulse. *IEEE Trans. Veh. Technol.* **2023**, *72*, 5809–5823. [CrossRef]
141. Liang, J.; Gan, Y.; Yao, M. Numerical analysis on the aging characteristics of a $LiFePO_4$ battery: Effect of active particle sizes in electrodes. *J. Energy Storage* **2023**, *67*, 107546. [CrossRef]
142. Parmananda, M.; Vishnugopi, B.S.; Garg, H.; Mukherjee, P.P. Underpinnings of Multiscale Interactions and Heterogeneities in Li-Ion Batteries: Electrode Microstructure to Cell Format. *Energy Technol.* **2023**, *11*, 2200691. [CrossRef]
143. Yang, X.G.; Wang, C.Y. Understanding the trilemma of fast charging, energy density and cycle life of lithium-ion batteries. *J. Power Sources* **2018**, *402*, 489–498. [CrossRef]
144. Duan, X.; Li, B.; Li, J.; Gao, X.; Wang, L.; Xu, J. Quantitative Understanding of Lithium Deposition-Stripping Process on Graphite Anodes of Lithium-Ion Batteries. *Adv. Energy Mater.* **2023**, *13*, 2203767. [CrossRef]
145. Zoerr, C.; Sturm, J.J.; Solchenbach, S.; Erhard, S.V.; Latz, A. Electrochemical polarization-based fast charging of lithium-ion batteries in embedded systems. *J. Energy Storage* **2023**, *72*, 108234. [CrossRef]
146. Chen, B.-R.; Kunz, M.R.; Tanim, T.R.; Dufek, E.J. A machine learning framework for early detection of lithium plating combining multiple physics-based electrochemical signatures. *Cell Rep. Phys. Sci.* **2021**, *2*, 100352. [CrossRef]
147. Weddle, P.J.; Kim, S.; Chen, B.-R.; Yi, Z.; Gasper, P.; Colclasure, A.M.; Smith, K.; Gering, K.L.; Tanim, T.R.; Dufek, E.J. Battery state-of-health diagnostics during fast cycling using physics-informed deep-learning. *J. Power Sources* **2023**, *585*, 233582. [CrossRef]
148. Lei, S.; Zeng, Z.; Liu, M.; Zhang, H.; Cheng, S.; Xie, J. Balanced solvation/de-solvation of electrolyte facilitates Li-ion intercalation for fast charging and low-temperature Li-ion batteries. *Nano Energy* **2022**, *98*, 107265. [CrossRef]
149. Persson, K.; Hinuma, Y.; Meng, Y.S.; der Van Ven, A.; Ceder, G. Thermodynamic and kinetic properties of the Li-graphite system from first-principles calculations. *Phys. Rev. B* **2010**, *82*, 125416. [CrossRef]
150. Chen, X.; Yao, N.; Zeng, B.-S.; Zhang, Q. Ion–solvent chemistry in lithium battery electrolytes: From mono-solvent to multi-solvent complexes. *Fundam. Res.* **2021**, *1*, 393–398. [CrossRef]
151. Yamada, Y.; Furukawa, K.; Sodeyama, K.; Kikuchi, K.; Yaegashi, M.; Tateyama, Y.; Yamada, A. Unusual Stability of Acetonitrile-Based Superconcentrated Electrolytes for Fast-Charging Lithium-Ion Batteries. *J. Am. Chem. Soc.* **2014**, *136*, 5039–5046. [CrossRef] [PubMed]
152. Gao, H.; Yan, Q.; Holoubek, J.; Yin, Y.; Bao, W.; Liu, H.; Baskin, A.; Li, M.; Cai, G.; Li, W.; et al. Enhanced Electrolyte Transport and Kinetics Mitigate Graphite Exfoliation and Li Plating in Fast-Charging Li-Ion Batteries. *Adv. Energy Mater.* **2023**, *13*, 2202906. [CrossRef]
153. Yue, X.; Zhang, J.; Dong, Y.; Chen, Y.; Shi, Z.; Xu, X.; Li, X.; Liang, Z. Reversible Li Plating on Graphite Anodes through Electrolyte Engineering for Fast-Charging Batteries. *Angew. Chem. Int. Ed.* **2023**, *62*, e202302285. [CrossRef]
154. Shuai, Y.; Zhang, Z.; Chen, K.; Lou, J.; Wang, Y. Highly stable lithium plating by a multifunctional electrolyte additive in a lithium-sulfurized polyacrylonitrile battery. *Chem. Commun.* **2019**, *55*, 2376–2379. [CrossRef]
155. Jeong, Y.T.; Shin, H.R.; Lee, J.; Ryu, M.-H.; Choi, S.; Kim, H.; Jung, K.-N.; Lee, J.-W. Insight into pulse-charging for lithium plating-free fast-charging lithium-ion batteries. *Electrochim. Acta* **2023**, *462*, 142761. [CrossRef]

156. An, J.; Zhang, H.; Qi, L.; Li, G.; Li, Y. Self-Expanding Ion-Transport Channels on Anodes for Fast-Charging Lithium-Ion Batteries. *Angew. Chem. Int. Ed.* **2022**, *61*, e202113313. [CrossRef]
157. Yang, J.; Li, Y.; Mijailovic, A.; Wang, G.; Xiong, J.; Mathew, K.; Lu, W.; Sheldon, B.W.; Wu, Q. Gradient porosity electrodes for fast charging lithium-ion batteries. *J. Mater. Chem. A* **2022**, *10*, 12114–12124. [CrossRef]
158. Yim, T.; Woo, S.-G.; Lim, S.H.; Cho, W.; Song, J.H.; Han, Y.-K.; Kim, Y.-J. 5V-class high-voltage batteries with over-lithiated oxide and a multi-functional additive. *J. Mater. Chem. A* **2015**, *3*, 6157–6167. [CrossRef]
159. Yao, Y.-X.; Chen, X.; Yao, N.; Gao, J.-H.; Xu, G.; Ding, J.-F.; Song, C.-L.; Cai, W.-L.; Yan, C.; Zhang, Q. Unlocking Charge Transfer Limitations for Extreme Fast Charging of Li-Ion Batteries. *Angew. Chem. Int. Ed.* **2023**, *62*, e202214828. [CrossRef]
160. Nan, B.; Chen, L.; Rodrigo, N.D.; Borodin, O.; Piao, N.; Xia, J.; Pollard, T.; Hou, S.; Zhang, J.; Ji, X.; et al. Enhancing Li^+ Transport in NMC811||Graphite Lithium-Ion Batteries at Low Temperatures by Using Low-Polarity-Solvent Electrolytes. *Angew. Chem.* **2022**, *134*, e202205967. [CrossRef]
161. Logan, E.R.; Dahn, J.R. Electrolyte Design for Fast-Charging Li-Ion Batteries. *Trends Chem.* **2020**, *2*, 354–366. [CrossRef]
162. Lei, S.; Zeng, Z.; Cheng, S.; Xie, J. Fast-charging of lithium-ion batteries: A review of electrolyte design aspects. *Battery Energy* **2023**, *2*, 20230018. [CrossRef]
163. Berhaut, C.L.; Porion, P.; Timperman, L.; Schmidt, G.; Lemordant, D.; Anouti, M. LiTDI as electrolyte salt for Li-ion batteries: Transport properties in EC/DMC. *Electrochim. Acta* **2015**, *180*, 778–787. [CrossRef]
164. Hall, D.S.; Eldesoky, A.; Logan, E.R.; Tonita, E.M.; Ma, X.; Dahn, J.R. Exploring Classes of Co-Solvents for Fast-Charging Lithium-Ion Cells. *J. Electrochem. Soc.* **2018**, *165*, A2365. [CrossRef]
165. He, D.; Lu, J.; He, G.; Chen, H. Recent Advances in Solid-Electrolyte Interphase for Li Metal Anode. *Front. Chem.* **2022**, *10*, 916132. [CrossRef]
166. Barlowz, C.G. Reaction of Water with Hexafluorophosphates and with Li Bis(perfluoroethylsulfonyl)imide Salt. *Electrochem. Solid-State Lett.* **1999**, *2*, 362. [CrossRef]
167. Freunberger, S.A.; Chen, Y.; Peng, Z.; Griffin, J.M.; Hardwick, L.J.; Bardé, F.; Novák, P.; Bruce, P.G. Reactions in the Rechargeable Lithium–O2 Battery with Alkyl Carbonate Electrolytes. *J. Am. Chem. Soc.* **2011**, *133*, 8040–8047. [CrossRef]
168. Milien, M.S.; Beyer, H.; Beichel, W.; Klose, P.; Gasteiger, H.A.; Lucht, B.L.; Krossing, I. Lithium Bis(2,2,2-trifluoroethyl)phosphate Li[O2P(OCH2CF3)2]: A High Voltage Additive for LNMO/Graphite Cells. *J. Electrochem. Soc.* **2018**, *165*, A2569. [CrossRef]
169. Diederichsen, K.M.; McShane, E.J.; McCloskey, B.D. Promising Routes to a High Li^+ Transference Number Electrolyte for Lithium Ion Batteries. *ACS Energy Lett.* **2017**, *2*, 2563–2575. [CrossRef]
170. Logan, E.R.; Tonita, E.M.; Gering, K.L.; Li, J.; Ma, X.; Beaulieu, L.Y.; Dahn, J.R. A Study of the Physical Properties of Li-Ion Battery Electrolytes Containing Esters. *J. Electrochem. Soc.* **2018**, *165*, A21. [CrossRef]
171. Qu, Z.G.; Jiang, Z.Y.; Wang, Q. Experimental study on pulse self–heating of lithium–ion battery at low temperature. *Int. J. Heat Mass Transf.* **2019**, *135*, 696–705. [CrossRef]
172. Zhang, G.; Wei, X.; Han, G.; Dai, H.; Zhu, J.; Wang, X.; Tang, X.; Ye, J. Lithium plating on the anode for lithium-ion batteries during long-term low temperature cycling. *J. Power Sources* **2021**, *484*, 229312. [CrossRef]
173. Qin, Y.; Zuo, P.; Chen, X.; Yuan, W.; Huang, R.; Yang, X.; Du, J.; Lu, L.; Han, X.; Ouyang, M. An ultra-fast charging strategy for lithium-ion battery at low temperature without lithium plating. *J. Energy Chem.* **2022**, *72*, 442–452. [CrossRef]
174. Wu, Y.; Long, X.; Lu, J.; Wu, Y.; Zhou, R.; Liu, L. Effect of temperature on the high-rate pulse charging of lithium-ion batteries. *J. Electroanal. Chem.* **2022**, *922*, 116773. [CrossRef]
175. Katzer, F.; Mößle, P.; Schamel, M.; Danzer, M.A. Adaptive fast charging control using impedance-based detection of lithium deposition. *J. Power Sources* **2023**, *555*, 232354. [CrossRef]
176. Shen, K.; Wang, Z.; Bi, X.; Ying, Y.; Zhang, D.; Jin, C.; Hou, G.; Cao, H.; Wu, L.; Zheng, G.; et al. Magnetic Field–Suppressed Lithium Dendrite Growth for Stable Lithium-Metal Batteries. *Adv. Energy Mater.* **2019**, *9*, 1900260. [CrossRef]
177. Dong, J.; Dai, H.; Wang, C.; Lai, C. Uniform lithium deposition driven by vertical magnetic field for stable lithium anodes. *Solid State Ion.* **2019**, *341*, 115033. [CrossRef]
178. Asenbauer, J.; Eisenmann, T.; Kuenzel, M.; Kazzazi, A.; Chen, Z.; Bresser, D. The success story of graphite as a lithium-ion anode material—Fundamentals, remaining challenges, and recent developments including silicon (oxide) composites. *Sustain. Energy Fuels* **2020**, *4*, 5387–5416. [CrossRef]
179. Sander, J.S.; Erb, R.M.; Li, L.; Gurijala, A.; Chiang, Y.M. High-performance battery electrodes via magnetic templating. *Nat. Energy* **2016**, *1*, 16099. [CrossRef]
180. Parikh, D.; Li, J. Bilayer hybrid graphite anodes via freeze tape casting for extreme fast charging applications. *Carbon* **2022**, *196*, 525–531. [CrossRef]
181. Kalnaus, S.; Livingston, K.; Hawley, W.B.; Wang, H.; Li, J. Design and processing for high performance Li ion battery electrodes with double-layer structure. *J. Energy Storage* **2021**, *44*, 103582. [CrossRef]
182. Ruan, H.; Jiang, J.; Sun, B.; Su, X.; He, X.; Zhao, K. An optimal internal-heating strategy for lithium-ion batteries at low temperature considering both heating time and lifetime reduction. *Appl. Energy* **2019**, *256*, 113797. [CrossRef]
183. Das, S.; Mohammad, B.; Navidi, S.; Sarkar, A.; Hu, C.; Shrotriya, P. Physics-Based State of Health Prediction of Lithium-Ion Battery during Fast Charging. *ECS Meet. Abstr.* **2024**, *MA2024-01*, 469. [CrossRef]
184. Goel, V.; Chen, K.-H.; Dasgupta, N.P.; Thornton, K. Optimization of laser-patterned electrode architectures for fast charging of Li-ion batteries using simulations parameterized by machine learning. *Energy Storage Mater.* **2023**, *57*, 44–58. [CrossRef]

185. Karati, A.; Gargh, P.P.; Paul, S.; Das, S.; Shrotriya, P.; Nlebedim, I.C. Materials recovery from NMC batteries with water as the sole solvent. *J. Environ. Manag.* **2024**, *366*, 121710. [CrossRef]
186. Sarkar, A.; Shrotriya, P.; Nlebedim, I.C. Electrochemical-driven green recovery of lithium, graphite and cathode from lithium-ion batteries using water. *Waste Manag.* **2022**, *150*, 320–327. [CrossRef]